ENCAPSULATION OF FLUORINATED NANOPARTICLES AS POTENTIAL OFF/ON PROBE FOR ^{19}F MRI

Elena Pérez Jiménez

Master in Synthetic and Industrial Chemistry

Master'sdissertation

September 2017

Dra. Mónica Carril García, IkerbasqueResearcher, hace constar que el trabajo titulado “Encapsulation of fluorinatednanoparticles as potential off/onprobefor ^{19}F MRI” que presenta Elena Pérez para la obtención de los 30 créditos del Trabajo Fin de Máster en Química Sintética e Industrial, ha sido realizado bajo mi dirección en los laboratorios de CIC biomaGUNE.

Y considerando que reúne los requisitos necesarios, autorizamos su presentación en la UPV/EHU, en Donostia a 14 de Septiembre de 2017.

Acknowledge

The present work took place in the group of Bioengineered Particles at CIC biomaGUNE (Center for Cooperative Research in Biomaterials), under Dr. **MónicaCarril** (Ikerbasque Research Fellow) which has been the mentor of present work and such inspiring person. I wish to express my deepest gratitude to her for this highly professional guidance and numerous inspiring discussions. In addition to her scientific brilliance, I especially appreciate her dedication pushing further when was necessary and giving breath when moments turn complicate.

Many thanks to my laboratory coworker's team: Pilar, Jorge, Mona, Carolina and Lorena. We have created our particularly family. Extraordinary people who are always helpful, handy, good friends and specially patients when stressing moments came up.

Family and friends endless list who share my life and make it a sense. They support me always with love and sincerity. Lucky me I got them in my life.

Finally, I want to thanks You for your love. The strength that makes me wake up every single day. You are the reason to be better person and surpass myself personally and professionally. There is no better love which gives meaning the person who I am.

Table of Content

List of Abbreviations

Abs: Absorbance

AuNP: Gold nanoparticle

CBD: Collagen-binding domain

dc: Core diameter

dh: Hydrodynamic diameter

DLS: Dynamic Light Scattering

ECM: Extracellular matrix

EDC: Ethylcarbodiimide hydrochloride

EE: Encapsulation Efficiency

equiv: Equivalent

GA: Glutaraldehyde

ICP-MS: Inductively coupled plasma mass spectrometry

MRI: Magnetic Resonance Imaging

MSN: Mesoporous silica nanoparticles

NMR: Nuclear Magnetic Resonance

PEG: Polyethylene glycol

PFCs: Perfluorocarbons

PRE: Paramagnetic Relaxation Enhancement

MMPs: Metalloproteinases

Mw: Molecular weight

NHS: N-Hydroxysuccinimide

NPs: Nanoparticles

PdI: Polidispersity index

pI: Isoelectric point

ppm: Parts per million

RT: Room temperature.

rpm: Revolutions per Minute

TEM: Transmission Electron Microscopy

UV-Vis: Ultraviolet Visible

vs. :versus

1. Introduction

Magnetic resonance imaging (MRI) has been recognized as a powerful and intrinsically non-invasive methodology for diagnosis. At the same time MRI is not associated to radioactivity problems and hence it is considered safe. Getting profit from high resolution, anatomical MR Imaging provides 3D tomography none invasively in living systems.

MRI is based on Nuclear Magnetic Resonance (NMR). On the one hand, medical field employs magnetic resonance imaging (MRI), a multidimensional NMR imaging technique, for diagnostic purposes. For many diseases, ^{1}H MRI has become the main modality of choice for the medical experts because it images water from inside the body. On the other hand, chemists have also largely exploited the NMR technique. They also contribute to magnetic resonance imaging field by designing contrast agents and reporter molecules based on relaxation of hydrogen atoms presents in water media.

Relaxation times of H atoms under magnetic field differ due to their surrounding atmosphere or because a restrictive mobility of water molecules. The difference between relaxation times is displayed as different signal intensity per voxel in MRI giving rise to an image with regions of different contrast.

Indeed, ^{1}H MRI has been extensively used due to the fact that adult human body contains about 50 to 65 per cent of water in average. Certainly, it is an interesting modality due to its good special resolution and also because of its reasonable sensibility towards contrast agent detection. Nonetheless, the intense proton background causes sometimes insufficient discrimination of damaged tissues from healthy ones.[1] This lack creates the necessity to explore new approaches such as the use of contrast agents or the use of heteronucleus MRI to enhance the contrast.

Probe's imaging relaxation time is a meaningful parameter to take into account to understand ^{1}H MRI probes classification in MRI. Probes altering

[1]Oishi, M.; Sumitani, S.; Nagasaki, Y. *BioconjugateChem*. **2007**, 18, 1379-1382.

T_1 and T_2 relaxation times of surrounding water in the body offer brighter and darker images, respectively.

An important advancement in the heteronucleus MRI as complementary technique to proton based MRI, is the fluorine 19 based MRI (**^{19}F MRI)**. ^{19}F MRI may be capable of producing high-contrast in vivo images, since there is no endogenous ^{19}F in the body that might be a source of background noise.[2]

Integrating these two imaging modalities (^{1}H and ^{19}F MRI), one can take advantages of both to identify and diagnose pathologies more accurately and robustly. In addition, common drugs include a fluorine atom, therefore fluorine is largely present in drug based treatments of numerous diseases, thus they are obvious candidates to apply this ^{19}F MRI technique.[3] In other cases, a fluorine atom may be added as a simple tracking molecule to interrogate some parameter, such as pO_2[4], pH[5] or gene activity.[6]

^{19}F has a nuclear spin of ½ and a gyromagnetic ratio (γ) of 40.05 MHz/T.[7] Note that ^{19}F is the only stable isotope of fluorine, it is 100 % naturally abundant and has magnetic resonance sensitivity nearly as high as that of proton. The NMR sensitivity of ^{19}F is 0.83 relative to ^{1}H.[8]

The high gyromagnetic ratio (*γ)* is only about 6 % lower than that of proton, and it generally allows the use of existing proton NMR instrumentation with minimum of component adjustments.

The ^{19}F signal provides an opportunity to image body organs which lack water where contrast ^{1}H MRI is handicapped by missing signal (e.g. lungs).[9]

---

[2]Tirotta, I.; Dichiarante, V.; Pigliacelli, C.; Cavallo, G.; Terraneo, G.; Bombelli, F. B.; Metrangolo, P.; Resnati, G. Chem. Rev. **2015**, 115, 1106-1129.
[3] Kirk, K.L. *J. Fluorine Chem* .**2006**, 127, 1013-1029.
[4] Thomas, S.R.; Millard, R.W.; Pratt, R.G.; Shiferaw, Y.; Samaratunga, R.C. *Art. Cells, Blood Subs., and Immob. Biotech*. **1994**, 22, 1029-1042.
[5]Preslar, A.T.; Tantakitti, F.; Park, K.; Zhang, S.; Stupp, S.I.; Meade, T.J. ACS Nano. **2016**, 10, 7376-7384.
[6]Gambhir, S.S.; Barrio, J.R.; Herschman, H.R.; Phelps, M.E. *Nucl. Med. Biol*. **1999**, 26, 481-490.
[7] Yu, J.; Kodibagkar, V.D.; Cui, W.; Mason, R.P. *Curr. Med. Chem*. **2005**, 12, 819-848.
[8] Ruiz-Cabello, J.; Barnett, B.P.; Bottomley, P.A.; Bulte, J.W.M. NMR Biomed. **2011**, 24, 114-129.
[9]Flögel, U.; Ding, Z.; Hardung, H.;Jander, S.; Reichmann, G.; Jacoby, C.; Schubert, R.; Schrader, J. *Circulation*. **2008**, 118, 140-148. / Fox, M.S.; Gaudet, J.M.; Foster, P.J. *Magn. Reson. Insights.***2015**, 8, 53-67.

Because nanoparticles provide with new properties and behave differently than small molecules it is possible to design new applications such as their use as contrast agents.

Since there is no endogenous ^{19}F signal, there is always the need to introduce an external fluorine labelled probe in order to obtain an image. Because there is no interference from image background, all which is displayed on ^{19}F MRI is directly proportional to the probe concentration, allowing an absolute quantification (non relative).

Frequently employed ^{19}F probes are based on perfluorocarbons (PFCs). These are hydrocarbons wherein al C-H bonds have been replaced by C-F bonds, which have solubility and stability issues and often multiple signals in ^{19}F NMR which lead to artifacts in MRI.

Hence, nanomaterials are an excellent alternative for currently in use fluorine based MRI probes. Some of the earliest biomedical applicationsof ^{19}F NMR used fluorine labelled substrates to explore enzymatic activity and protein structures. To obtain detectable signals, spectra, or images, sufficient fluorinated probe must be administered, though the probe's concentration in studies of living organisms should be as low as possible to avoid physiological perturbations or toxic side effects (Figure 1.1).

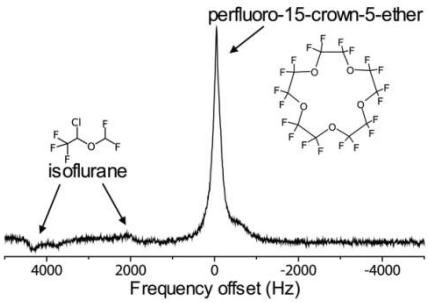

Figure 1.1: ^{19}F NMR PFCs examples of isoflurane and perfluoro-15-crown-5-ether displaying the importance of the F load on peak intensity.

However, in order to achieve a good quality of image comparable to those obtained with ^{1}H MRI (or at least acceptable), a high load of fluorine atoms is required. Hence, the main challenge in this field is to introduce high fluorine

amount in a probe, but conquer fluorine insolubility in water for medical applications, which is not easy due to the intrinsic hydrophobicity conferred by fluorine atoms.

Recently, our research group[10] has designed a novel nanostructure that overcomes the intrinsic hydrophobic nature of fluorinated compounds by using a long PEG chain. Ensuring ligand mobility due to PEG structure also ensures a successfully colloidal stable system in water and a good signal in ^{19}F MRI.

Additionally these nanoparticles display a sharp single ^{19}F NMR signal which could also be imaged by ^{19}F MRI.[10] The lack of background signal allows for the absolute quantification of the signal that is directly proportional to the probe concentration. Synthesis of nanoparticles tagged with fluorinated ligands resonating all of them at the same frequency is achieved only through chemical equivalent fluorine atoms on the ligands. In this case employing symmetrical fluorinated probe they have sorted out signal's splitting issue (Figure 1.2).

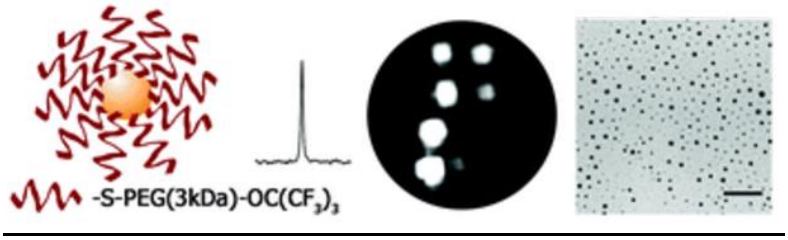

Figure 1.2: Nanostructure designed by our research group.

Due to the lack of background signal existing in ^{19}F MRI, fluorinated probes have become excellent candidates for OFF/ON probe systems, which consist of probes that are silent in MRI until a selected trigger activates the signal. These types of probes are interesting because they provide additional functional information on biological processes in real time.[11]

Further, fluorine in vivo is present mostly in the form of solid fluorides, in bones and teeth, for this reason endogenous fluorine has a very short T_2

[10]Michelena, O.; Padro, D.; Carrillo-Carrion, C. del Pino. P.; Blanco, J.; Arnaiz, B.; Parak, W.J.; Carril, M. *Chem. Commun.* **2017**, 53, 2447-2450.

relaxation time on MRI and the resulting signal is below the limits of MRI detection in most biological systems of interest.[11]

As mentioned before, OFF/ON, activable or smart probes are systems, where signal is OFF temporarily and then it is activated to an ON state by an external incentive. All activatable probes share the same feature: an external **stimulus is needed**.

A variety of stimuli-sensitive ^{19}F probes have been developed so far. Probes reported on the literature can be classified based on their trigger, mainly by pH, redox atmospheres or enzyme responsive. Upon stimulation, these designed molecules turn into an ON state in a specific environment.

For instance, there are pH responsive MRI probes which are suitable for tumor cells detection due to the fact that pH values within tumor cells range from 5.5 to 6.8, being these values lower than those in healthy cells. In many cases detection of pH by ^{19}F MRI pH responsive probes is based on the mobility of the fluorinated probe within a polymeric matrix.

Selectively designed matrixes get protonated under specific pH environment, then the hydration leads to gel swelling allowing fluorine mobility and hence activating the MRI signal.

Chen[12] et al. have designed a nanosized pH triggered probe based on the encapsulation of a fluorinated probe into mesoporous silica nanoparticles (MSN) cavities that were capped with gold nanoparticles. Those gold nanoparticles were bond onto silica's surface by hydrazone linkage, which is pH sensitive. At neutral pH 7.4 the hydrazone linkers remain intact, thus, pores are blocked with AuNPs. At pH lower than 6 hydrazone's bond goes through a hydrolysis reaction releasing gold nanoparticles onto the surface, thus, opening the gate to release C_6F_6 contrast agent turning ON the smart probe (Figure 1.3).

[11]Carril, M. *J. Mater. Chem. B.***2017**, 5, 4332-4347.
[12] Chen, S.; Yang, Y.; Li, H.; Zhou, X.; Liu, M. *Chem. Commun.***2014**, 50, 283-285.

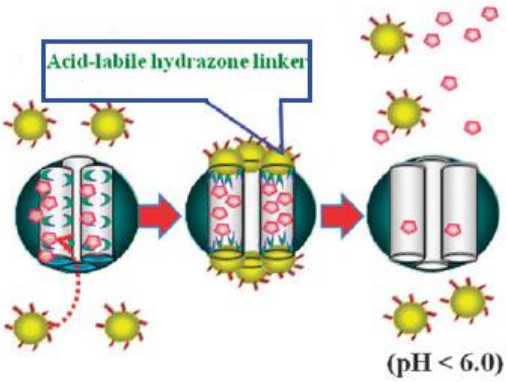

Figure 1.3: Chen's pH trigger bioprobe design (Cylinders are MSNs, Yellow spheres are gold nanoparticles blocking surface cavities. Pink hexagons are C_6F_6 fluorine contrast agent)

Another type of OFF/ON probes are redox responsive MRI probes, which are suitable for tumor cell detection because of their reducing environment due to the presence of glutathione. ^{19}F MRI probes play with paramagnetic metals in the neighborhood of ^{19}F nuclei by PRE (paramagnetic relaxation enhancement). If the metal is nearby ^{19}F nuclei this is deactivated on MRI, besides, when the metal is faraway from^{19}F nuclei, then^{19}F signal becomes active on MRI. This effect allows reversible switch OFF/ON of fluorine probe.

Hypoxia is an oxygen deficiency condition experienced in solid tumor cancers and also in other pathologies. Que[13] et al. have developed a copper based probe where Cu(II)/Cu(I) pairs are used to switch OFF and ON the fluorine signal based on Paramagnetic Relaxation Enhancement (PRE) effect.

In this case, the molecule reported is a chelate with a fluorinated side chain. When fluorine atoms are close to Cu(II) are inactive on ^{19}F MRI. However, once Cu (II) is reduced to Cu (I) by hypoxic cells ^{19}F MRI signal is turned ON (Figure 1.4).

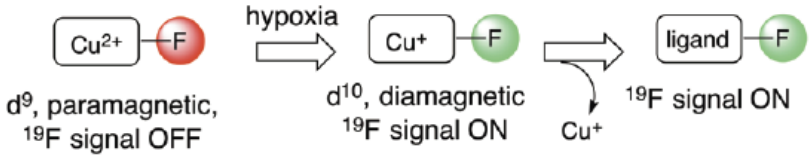

Figure 1.4: Schematic representation of Que's bioresponisve probe regulated by PRE effect.

[13]Xie, D.; King, T.L.; Banerjee, A.; Kohli, V.; Que, E.L. *J. Am. Chem. Soc.,***2016**, 138, 2937-2940.

Enzyme responsive MRI probes are one of the main areas of interest, being enzymes an indicator of pathologies progression due to its deregulation and also a disease symptom indicator.

Yuan[14] et al. have designed a fluorine probe for imaging caspase 3/7 enzymatic activity in vivo which is a cellular apoptosis indicator studied in tumor therapy. The probe design is based on trapping fluorinated compounds in nanoparticles formed by glutathione induced self assembly of DVED peptide, which is a substrate for caspase 3/7, as the ^{19}F MRI OFF state. Then, in the presence of caspase 3/7, DVED peptide gets digested and disassembles the macrostructure releasing the fluorinated probe and hence activating the ON state. The in vivo test has been carried out on zebrafish model (Figure 1.5).

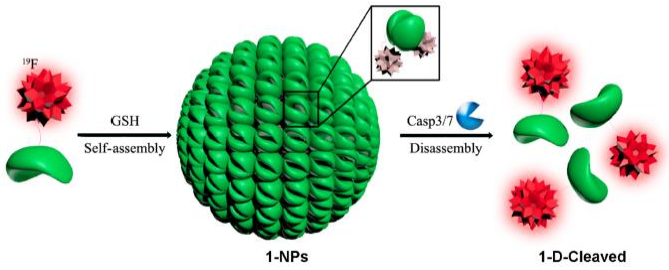

Figure 1.5: Yuan's smart probe design.

In the present work, we have designed and synthesized a **novel probe with potential application as enzyme responsive smart probe for ^{19}F MRI**. On this new approach, the target enzyme is metalloproteinase 9 (MMP-9) which has been strategically chosen as the trigger due to its role in several disease pathways.

Matrix metalloproteinases (MMPs) are involved in many physiological and pathological processes,[15] due to their ability to cleave and remodel components of surrounding tissues. MMPs may affect cell migration, differentiation, neovascularisation, wound healing, apoptosis, growth,

[14] Yuan, Y.; Sun, H.; Ge, S.; Wang, M.; Zhao, H.; Wang, L.; An, L.; Zhang, J.; Zhang, H.; Hu, B.; Wang, J.; Liang, G. *ACS Nano*, **2015**, 9, 761-768.
[15] Murphy, G.; Nagase, H.; *FEBS J,***2010**, 278, 2-15.

inflammatory process, urine cycleand many other actions within the body as tumorigenesis and other diseases.[16]

More than 20 classes of MMPs have been identified in humans, labelled from MMP-1 to MMP-28. MMPs are located onto cell surface where selectively degrade various components of extracellular matrix (ECM). Hence, MMPs play crucial roles in invasion and metastasis and regulate signalling pathways that control cell growth, survival, invasion, inflammation and angiogenesis.

High levels of MMP-2 and/or MMP-9 are found in breast, brain, ovarian, pancreas, colorectal, bladder, prostate and lung cancer and melanoma. Dysregulated MMP expressions is also observed in haematological malignancies.[12] MMPs also are present in cardiovascular field as in stroke, aneurism and atherosclerosis. Specifically MMP-2 (gelatinase A) and MMP-9 (gelatinase B) differ from most of the other MMPs in that they have a collagen-binding domain (CBD) within the catalytic domain (Figure 1.6). Furthermore, gelatinases generate or release bioactive molecules that influence tumour's progression.[12]

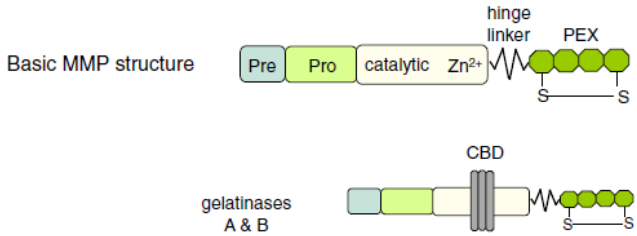

Figure 1.6: First, the general domain structure of MMP family; Pre: guides the MMP into the rough endoplasmic reticulum during synthesis; Pro: sustains the latency of MMP. The catalytic domain houses a highly conserved Zn^{2+} binding region; PEX: hemopexin-like-C-terminal Secondly the gelatinases contain the collagen binding domain (CBD) by Bauvois.[17]

There are several possible reasons for the failure of MMP's detection in the clinic. Firstly, most of the MMPs have dose-limiting musculoskeletal toxicity that limits efficacy. Secondly, the clinical trials were performed on patients with terminal-phase cancer, where several overlapping pathways

[16]Krizkova, S.; Zitka, O.; Masarik, M.; Adam, V.; Stiborova, M.;Eckschlager, T.; Chavis, G.J.; Kizek, R. *Trends Anal. Chem.***2011**, 30, 11.
[17]Bauvois, B. *BiochimBiophysActa.***2012**, 1825, 29-36.

come into play. Thirdly, the structural similarities of the various MMP's catalytic domains make it difficult to design probes for MMPs with high selectivity.[18]

Being gelatin the substrate for our MMP-9 and being also extensively reported on literature as a drug delivery vehicle, we believe gelatin nanoparticles can be an excellent system to be used as a carrier for fluorinated probes and at the same time act as a substrate for our trigger (MMP-9) constructing in this manner a MMP-9 responsive OFF/ON probe for ^{19}F MRI.

It isessential to understand the purpose of encapsulation and the mechanism for nanoparticles release for the rational design of encapsulated particles, from selection of the appropriate matrix material and formulation of capsule to obtain structures that protect the core and respond appropriately to the desired stimulus.

In the development process of a nanoparticle delivery system for *in vivo* application, biodegradability without toxic by products is one of the major claims. Collagen and gelatin have raised specific interest as promising delivery vehicle for controlled release of biomolecules such proteins, nucleotides and metal core nanoparticles as we are going to discuss further in the present work.

Due to collagen intrinsic protein structure with high number of different accessible functional groups, gelatin endows multiple modification opportunities for coupling of targeting ligands, crosslinkers, and shielding substances.

Utilizing MMPs as target for in-vivo imaging is a relatively young approach. Notwithstanding the extensive literature on this subject, there are no good imaging probes reported for MMP gelatinases detection.

Getting information about dynamic processes and functional information in real time through smart and bio-responsive probes is crucial to make a more specific diagnosis. We have explained several examples of OFF/ON contrast

[18]Overall, C.M.; Kleifeld, O.; Br. *J. Cancer*, **2006**, 94, 941-946.

agents. Ideally MRI detection would require an initial non-detectable probe (OFF state) to a detectable probe system (ON state) by contrast agent.

Spotlighting the present work in key points; firstly enzyme responsive probes on MRI imaging are potential biomarkers through trigger. Secondly, nanoparticles play an important role as delivery system. Lastly, metalloproteases are a potential trigger on gelatine substrates. So, **a novel ^{19}F MRI smart probe has been designed for potential OFF/ON detection of MMP-9.**

2. Objectives

The present work deals with the synthesis of fluorine labeled gold nanoparticles followed by their encapsulation in gelatin nanoparticles. The choice of gelatin is based on its role as substrate for gelatinases MMP enzymes (MMP-2/9). Hence, our hypothesis is that when our fluorine labeled NPs are encapsulated in gelatin the ^{19}F MRI signal would be OFF. The disassembly of the gelatin NPs triggered by its digestion by MMPs should lead to the turning ON of the signal (Figure 2.1). The specific goals are listed below:

1. Optimization of the synthesis and characterization of gelatin nanoparticles of 250-350 nm diameter.

2. Synthesis and characterization of fluorine-labeled gold nanoparticles, following already established procedures in our laboratory.

3. Design and optimization of an efficient encapsulation pathway for loading gelatin NPs with F-labeled Au NPs and characterization of the so-obtained materials.

4. Demonstrate via ^{19}F NMR that the signal of fluorine labeled gold nanoparticles is quenched by gelatin encapsulation (OFF state) as a validation of our design of a bioresponsibe probe.

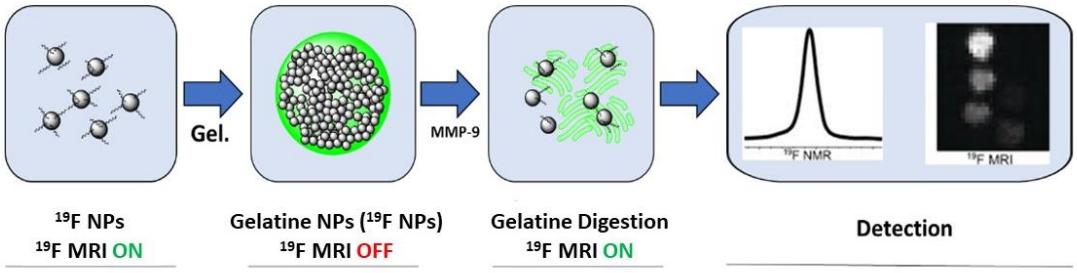

Figure 2.1: Schematic representation of our probe design and the main aim of the present work.

3. Results and Discussion

3.1. Gelatin nanoparticles' synthesis

In the present work, gelatin nanoparticles have been chosen as a promising vehicle due to theirbiocompatibility; ease of manipulation and also due to their potential to target matrix metalloproteinase 9 enzyme (MMP-9).

Collagen as an extracellular protein matrix is present in bones and tendons (90%) and skin where 50% of this matrix is collagen, which is the main way to obtain gelatin by denaturalization treatment of animal collagen (Figure 3.1). The amino acid composition of collagen and hence of gelatin is about 33% glycine, thus, Gly-X-Y represents the continually repeating amino acid sequence.

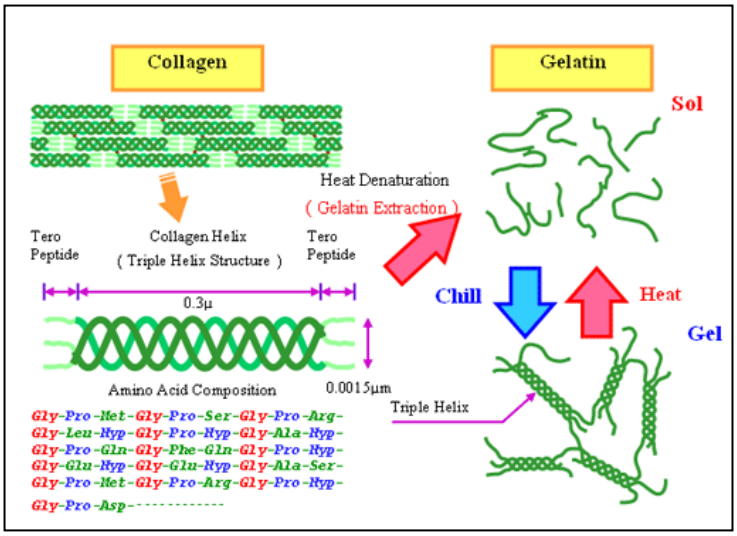

Figure 3.1: Structural transformation of collagen into gelatin.(http://imgur.com/TdOJOwh)

At the present work gelatin type A from porcine skin has been employed to conduct the synthesis and characterization of gelatin nanoparticles, which are intended to act as a trigger on the activatable bioprobe targeting MMP-9, also known as gelatinase enzyme.

Since molecular gelatin composition is heterogeneous, the preparation of homogeneous nanoparticles in size is challenging. Desolvation of the

commercial gelatin protein was chosen as the pathway to synthesize nanosized gelatin particles.

Gelatin is soluble in water in all its widespread of molecular weights as obtained from natural commercial sources. To achieve gelatin nanoparticles homogeneity in size, a narrow molecular weight (Mw) range is desired. According to literature, two step desolvation method consisting of adding a non solvent and then adjusting the pH to the pI of gelatin enables the preparation of homogeneous gelatin spheres.[19]

Based on our experience, the key to succeed in our gelatin nanoparticle synthesis is to work at a pH value higher than the first pKa of gelatin. In this situation, carboxyl groups will be mainly present as carboxylatesand will favor precipitation of gelatin nanoparticles in the desolvating solvent, usually acetone. Determination of optimum pH was one of the most challenging points. In our case, pH = 3 was selected as the best working conditions after several trials at different pH values between 2.5 and 4. This range was selected based on the fact that the majority of collagen aminoacids reach their first pKa between 2.5 and 4.

Once gelatin dissolved in water gets in contact with acetone or ethanol, the biggest molecular weight chains immediately precipitate. Acetone has been chosen as the desolvation solvent in our case due to the numerous reports that use acetone.[20] The water/acetone ratio in the first desolvation step is 1/1 (v/v) and the time the gelatin is allowed to precipitate after acetone addition (1 min in our case) will determine the amount and also the Mw range of the gelatin precipitate obtained. Hence, these are key factors to be controlled for synthetic reproducibility.

Then, once a narrow range of Mw has been obtained after the first desolvation step, a second desolvation step is required to form NPs by controlled dropwise addition of acetone, after which NPs are immediately formed as evidenced by the turbidity observed. Gelatin insolubility in acetone is the reason why protein chains fold on themselves. In this manner nanospheres

[19]Coester, C.J.; Langer, K.; Briesen, H.V.; Kreuter, J. *J. Microencapsulation,* **2000**, 17, 187-193.
[20]Gaihre, B.; Khil, M. S.; Lee, D. R.; Kim, H. Y. *Int. J. Pharm*. **2009**, 365, 180-189.

are spontaneously shaped. This kind of interaction is weak, thus the so-obtained nanoparticles will not remain stable over time unless crosslinked (Figure 3.2).

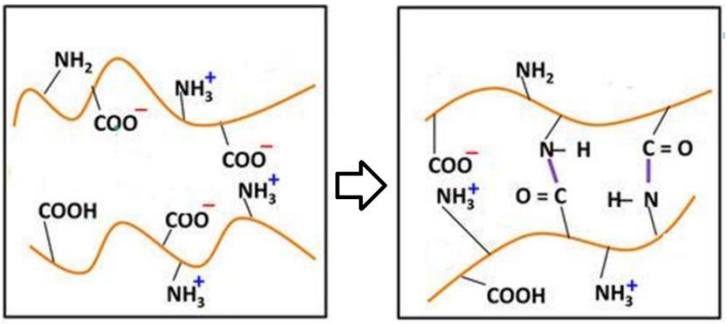

Figure 3.2: Gelatin polymer chain at pH = 3 on left. Gelatin chains already crosslinked by amidation bond on right side.

The most common crosslinker in gelatin nanoparticles formation is glutaraldehyde (GA)[21] but we chose EDC/NHS for biocompatibility, since GA is known to be toxic.[22]

Chemical crosslinking agents can be classified into non zero-length and zero length crosslinkers. Non zero-length agents introduce poly- and bifunctional crosslinkers into the network structure by bridging free amine groups (from lysine and hydroxylysine) or by free carboxylic acid residues (from glutamic and aspartic acid) of the protein molecules. Glutaraldehyde is widely used in literature. The disadvantage of these agents is that the crosslinkers are built into the biomaterial. These reactive and/or even toxic compounds may leach into the body upon biodegradation of the hydrogel.[23]

Zero-length crosslinkers do not imply incorporation of a foreign structure into the network. The most common pathway is by activating carboxylic acid residues to react with free amine residues, which resultsin the formation of an amide bond, ensuring that external compounds do not remain in the nanoparticles. Acyl azide method and the carbodiimide crosslinkings are

[21] Reis, C.P.; Neufeld, R.J.; Ribeiro, A.J.; Veiga, F. *NANOMED-NANOTECHNOL,* **2006**, 2, 8-21.
[22] Fürst, W.; Banerjee, A. *Ann. Thorac. Surg*., **2005**, 79, 1522-1528.
[23] Kuijpers, A.J.; Engbers, G.H.; Krijgsveld, J.; Zaat, S.A.J.; Dankert, J.; Feijen, J. Biomater. Sci. Polym. Ed., **2000**, 11, 3.

representative of this class of crosslinkers for gelatin or collagen substrates. Since toxic hydrazine is employed in the acyl azide linkage method,[24] carbodiimide pathway has been considered a safe bet in the present work (Scheme 3.1).

Since most of the methods reported in literature use GA, we needed to do an extensive optimization to achieve more or less monodisperse gelatin nanoparticles using EDC/NHS as crosslinking agents.[25]

The two crucial factors to control the results are the protein amount after the first desolvation step and the pH value before the second desolvation step. But also the amounts of crosslinker and addition rates are of high importance when we talk about size homogeneity, especially if later release of entrapped cargo and degradation kinetics are concerned.

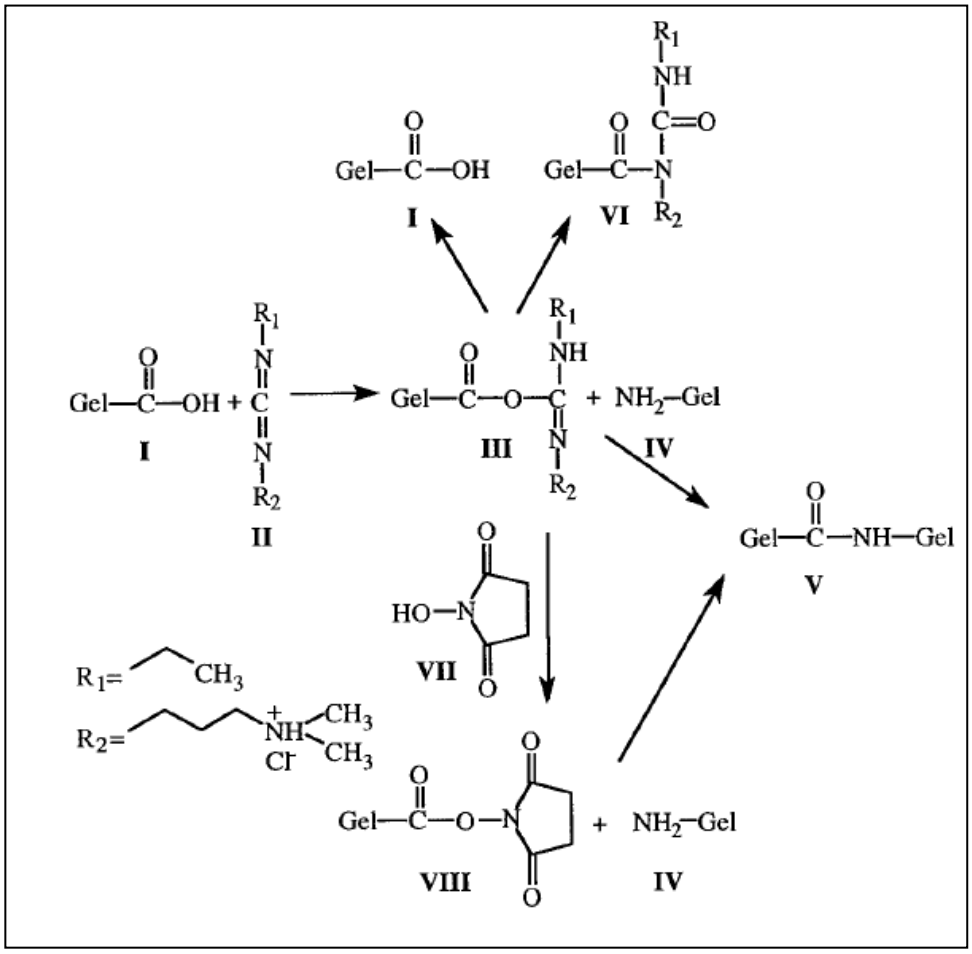

Scheme 3.1: EDC/NHS crosslinking reaction on gelatin.[26]

[24]PandurangaRao, K.; J. Biomater. Sci. Polym Ed, **1995**, 7, 623-645.
[25]Qazvini, N.T.; Zinatloo, S.; *J. Mater. Sci.*, **2011,** 22, 63-69.

Reported by Kuijpers et al., crosslinking of proteins with carbodiimide is generally considered to take place according to the mechanism on Scheme 3.1. Carbodiimide (II) activates carboxylic acid residues of aspartic and glutamic acid (I) resulting in the formation of O-acylisourea groups (III). Crosslinked compound (V) can be formed by nucleophilic attack of free amine groups of lysine and hydroxylysine residues (IV) on the activated carboxylic acid residues, with urea derivative as a leaving group. Possible secondary reactions of such linkage are hydrolysis of the O-acylisourea group, resulting in the formation of a carboxylic acid group (I), and rearrangement of the O-acylisourea group into a stable N-acylurea group (VI). The use of N-hydroxysuccinimide (NHS) (VII) in the crosslinking reaction gives an NHS activated carboxylic acid group (VIII), which is less susceptible to hydrolysis, and prevents rearrangement. All residues are water soluble, and can be effectively washed out of the gel after crosslinking.

There are a number of reports on the literature to prepare gelatin NPs mainly using GA as crosslinker and leading to nanoparticles of varied sizes depending on the reaction parameters employed. In our case, for encapsulation purposes we aimed at NPs of approximately 250 nm in diameter so that we could allocate a good number of gold nanoparticles inside but they are not excessively big for bioapplications. For this reason, we first needed to optimize all reaction parameters only with gelatin before testing encapsulation.

In addition, it has to be mentioned that robustness in reproducibility is challenging and can only be achieved by extremely methodic working conditions and accuracy.

Preliminary optimization from the group based on the protocol reported by Wong et al.[27] set the pavement for the initial conditions tested and after variation of few parameters we managed to obtain homogeneous gelatin NPs in size and in a reproducible manner.

---

[26]Kuijpers, A.J.; Engbers, G. H.M.; Krijgsveld, J.; Zaat, S. A. J.; Dankert, J.; Feijen, J. J. Biomater. Sci. PolymerEd, **2000**, 3, 225-243.

[27] Wong, C. Stylianopoulos, T. Cui, J.; Martin, J.; Chauhan, V.P.; Jiang, W.; Popovic, Z.; Jain, R.K.; Bawendi, M.G.; Fukumura, D. PNAS, **2010, 108, 2426-2431.**

The optimized parameters for the synthesis of gelatin nanoparticles are the following:

- Temperature reaction: 50ºC
- Stirring: 750 rpm
- pH= 3.00
- Acetone addition rate (2n desolvation step): 1 mL/min
- EDC/NHS ratio: 3.5:1, added in a 0.9 % aqueous solution.
- EDC/NHS solution addition rate: 0.1 mL/min
- 1 hour reaction time after EDC/NHS addition.

Work temperature has been established at 50 ºC due to sol-gel transition temperature of gelatin is at 35-40ºC. The fully optimized protocol for the synthesis of gelatin nanoparticles is described in detail in the materials and methods section and summarized in Scheme 3.2.

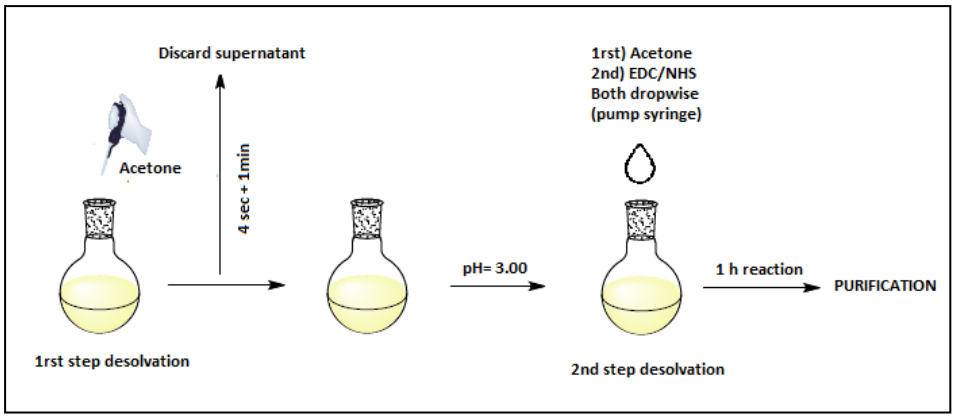

Scheme 3.2: Schematic representation of the workflow used to prepare gelatin nanospheres.

Considering the applicability of nanoparticles as a vehicle delivery system, size is a parameter to take into account. Quality control of the resulting nanoparticles is done by DLS (Dynamic Light Scattering) measurements. Size distribution of gelatin nanoparticles is determined by their PdI (polidispersity index), which in our case ranged between 0.3-0.1. PdI below 0.1 means that a highly monodisperse size distribution have been obtained. As an example of

DLS measurement of our gelatin nanoparticles, a size distribution plot by DLS is displayed on Figure 3.3.

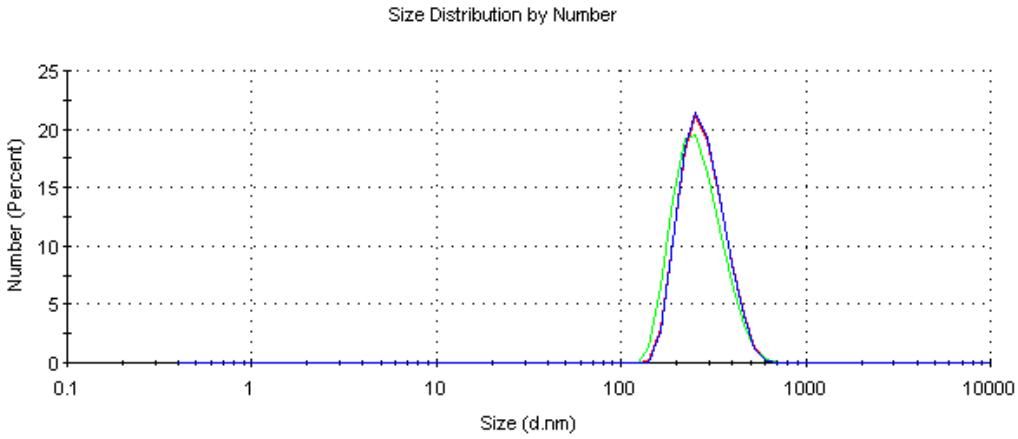

Figure 3.3: DLS distribution showing size by number of three measurements.

The Zetasizer software calculated 277.7 ± 6.30 nm by number as the mean size of these particles with a PdI of 0.09 ±0.06 (out of 3 measurements).

In addition, gelatin nanoparticles have been analyzed by TEM (Transmission Electron Microscopy) in order to visualize the particles and investigate their morphology. Uranyl acetate based negative stained samples analyzed by TEM revealed the sample as smooth spheres of 188.7 ± 36.1 nm size, as plotted in Figure 3.4. (Statistics displayed on Figure 3.5).

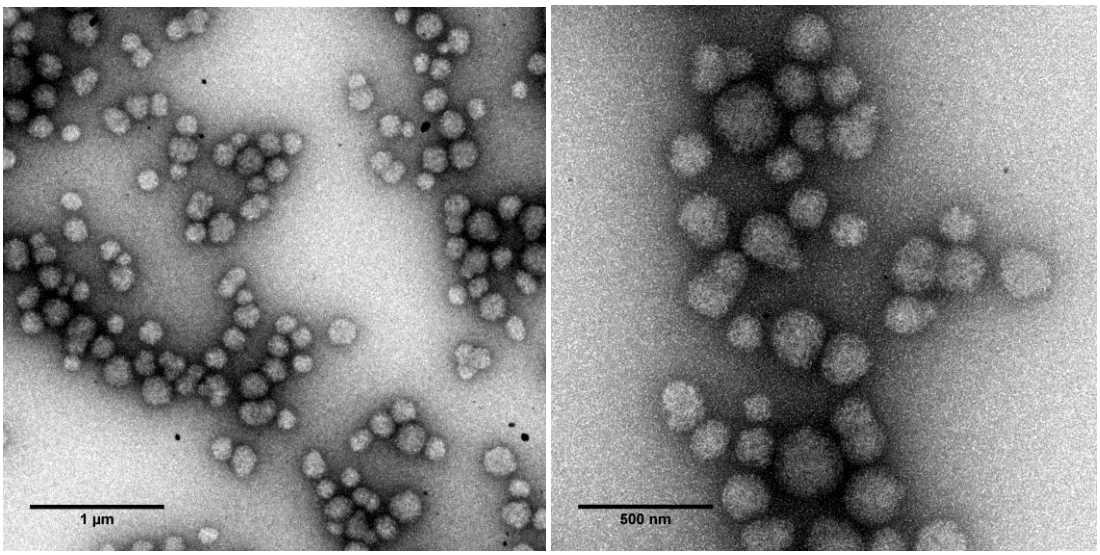

Figure 3.4: Gelatin nanospheres morphology shown by TEM micrographs.

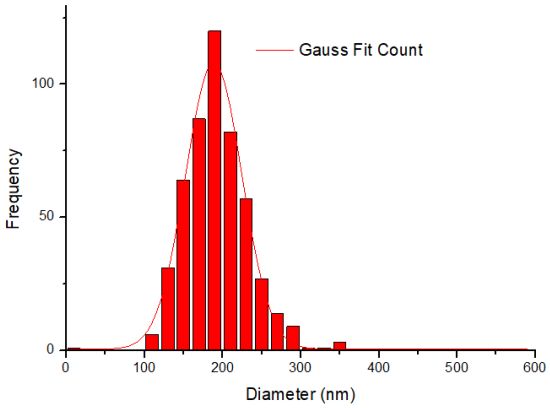

Figure 3.5: Histogram fitted to a Gaussian distribution of gelatin nanoparticles' size using Origin 8.5 software.

We were aware that a significant discrepancy could happen and should be seen between DLS distribution and TEM results according to the measurement principle of both analytical methods. This is because nanoparticles cannot be measured under equal conditions. Indeed, particles under DLS conditions have to be dispersed in a solvent, whereas TEM preparation sample requires drying the particles under vacuum conditions.

Hence, while DLS measures hydrodynamic diameter (d_h) of gelatin nanoparticles in solution, particles measured under the TEM suffer a shrinking in their diameter size by sample's dehydration.

Once gelatin parameters have been optimizedwe moved on to our next goal, that is, encapsulation of fluorinated gold nanoparticles to obtain a potentially activatable probe to image MMP-9 activity by ^{19}F MRI.

3.2. Synthesis of fluorine labeled gold nanoparticles.

Following with the research line of our group in which gold NPs are labeled with fluorinated ligands for potential ^{19}F MRI applications, five NPs with different degree of fluorination or methoxy groups were synthesized following the reported procedure.[10]

Such fluorinated gold NPs previously described by us are composed of an inorganic gold core and an organic shell. Such organic shell is based on polyethylene glycol (PEG) ligands due to their water solubility. Those PEG ligands have a thiol moiety for gold NP synthesis and are either modified with a methoxy group or a perfluorinated *tert*-butanol derivative. The methoxy modified NPs were selected as model NPs for preliminary optimization of the encapsulation process, although the main goal is the encapsulation of the fluorinated NPs. We already proved that the latter NPs are active in ^{19}F MRI (Figure 3.6).[10]

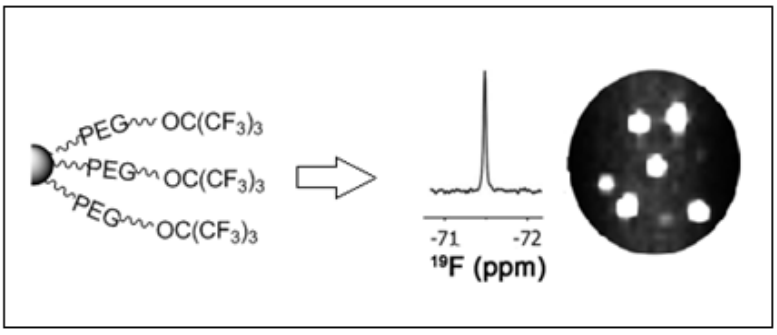

Figure 3.6: Fluorine labeled gold nanoparticles reported recently by our group.[10]

Methoxy functionalized PEG was commercially available but fluorinated PEG ligand was synthesizedin the laboratory as described by us and shown in Scheme 3.3.

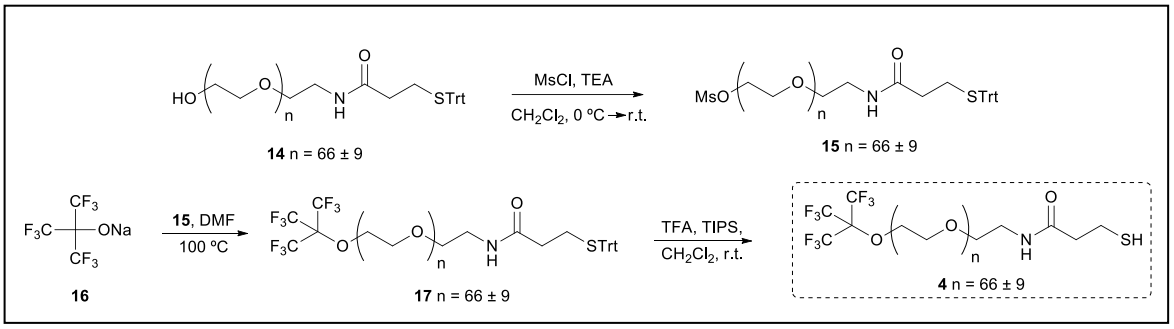

Scheme 3.3: Synthesis of fluorinated PEG ligand.

In addition, in order to test different encapsulation strategies, as it will be described below, NPs combining either fluorinated or methoxy PEG with commercially available carboxylated PEG derivative were synthesized. NPs were prepared following the established procedure by us consisting of chloroauric acid reduction by $NaBH_4$ in the presence of enough thiolated ligands to stabilized the so-obtained gold NPs.

As mentioned before, initially, surrogate NPs with a methoxy group instead of fluorine were prepared to pre-optimize encapsulation reaction. The amount of ligand used to stabilize each NP was set to 0.45 equivalents in total with respect to chloroauric acid, as it was already optimized in the laboratory. For mixtures of ligands, the 0.45 equivalent total value was maintained and the percentages shown in Table 3.1 are considering that 0.45 is the 100%. Synthetic procedure for our gold NP preparation is displayedin Scheme 3.4.

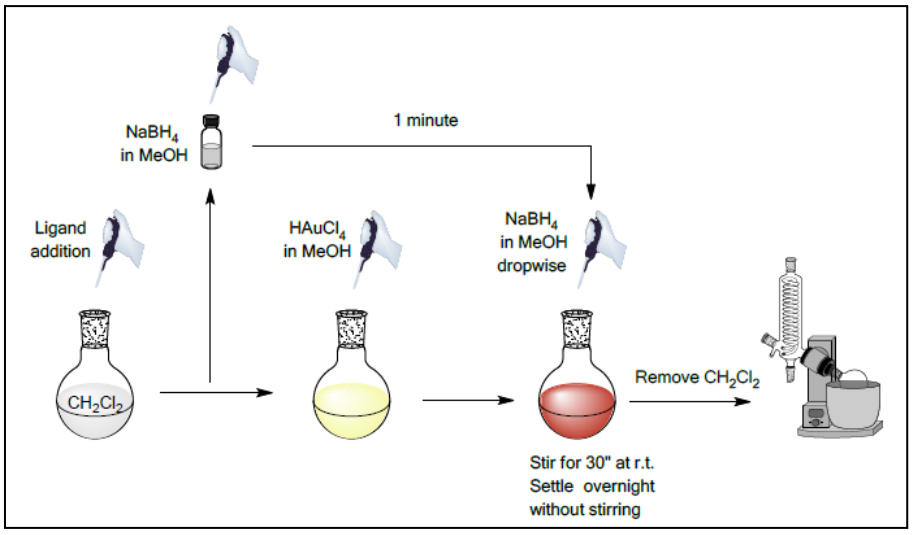

Scheme3.4: Schematic representation of the workflow used to prepare NP1-5.[10]

Table 3.1: Ligand ratio distribution onto gold nanoparticles surface

AuNPs	NP1	NP2	NP3	NP4	NP5
Ligand ratio	100% HS-PEG-OMe	75%HS-PEG-OMe 25% HS-PEG-CO_2H	100% HS-PEG-F	75%HS-PEG-F 25% HS-PEG-CO_2H	90% HS-PEG-F 25% HS-PEG-CO_2H

Transmission electron microscopy of NP cores

Transmission Electron Microscopy (TEM) analysis allows a direct measurement of the size and shape of NPs. The organic ligand shell typically does not provide sufficient electron contrast, and thus in TEM images only the inorganic part of the NPs can be seen. Also the state of agglomeration can be observed. Characterization of the gold core size was carried out only by transmission electron microscopy because DLS technique is imprecise for particles under 10 nm. We show in Figure 3.7 the TEM micrographs and size distributions of **NP1-5**. As expected for the synthetic methodology employed, the size of the so-obtained NPs is about 4 nm in diameter, as shown in Table 3.2.

NP1

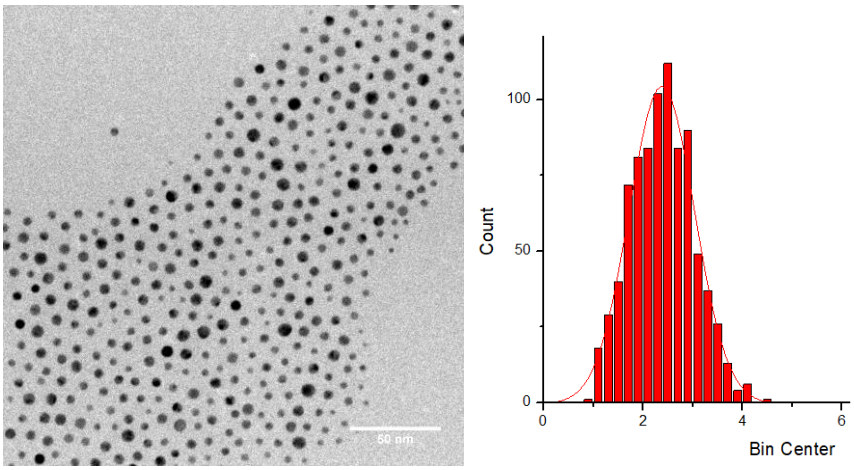

NP2

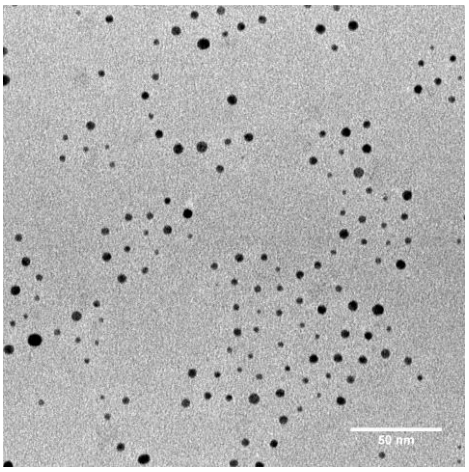
50 nm

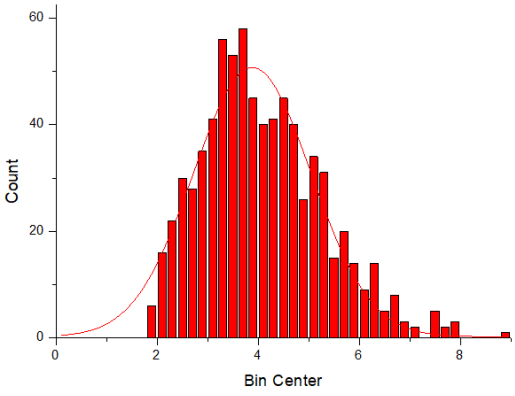
Count
Bin Center
0
20
40
60
0
2
4
6
8

NP3

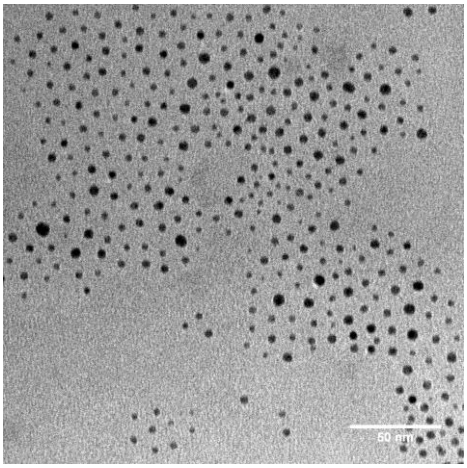
50 nm

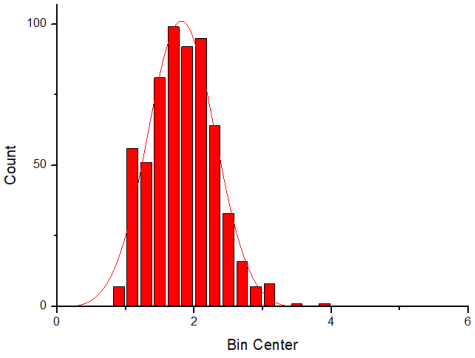
Count
Bin Center
0
50
100
0
2
4
6

NP4

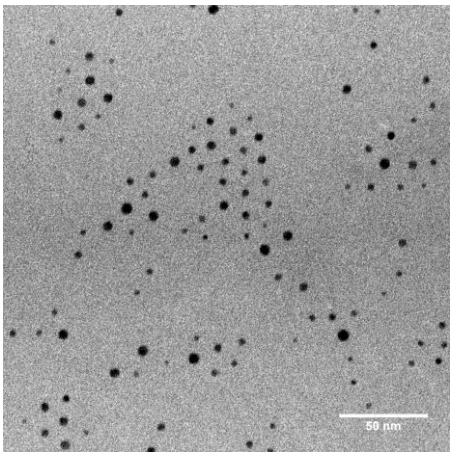
50 nm

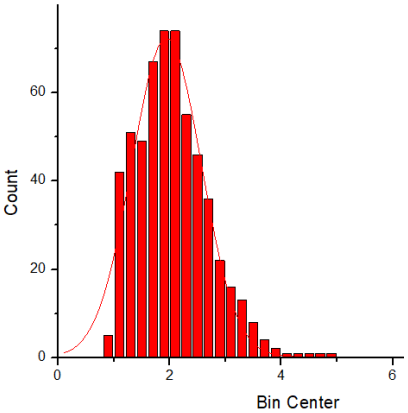
Count
Bin Center
0
20
40
60
0
2
4
6

NP5

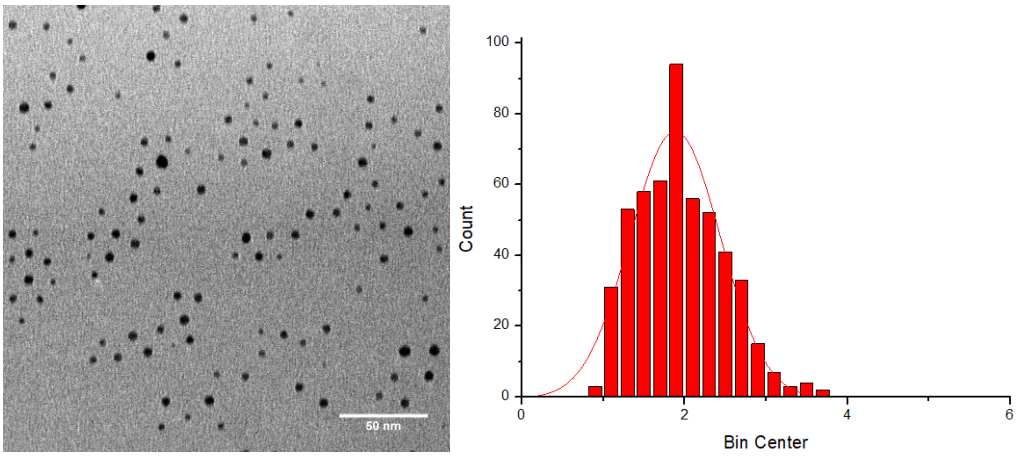

Figure 3.7: On the left side, TEM micrographs of each NP synthesized. On the right side, histograms with Gaussian distribution for each NP.

Table 3.2: TEM diameter size (nm) measured by Image J free software

	NP1	NP2	NP3	NP4	NP5
d_c(nm)	4.75 ± 0.66	3.89 ± 1.17	3.63 ± 0.49	3.88 ± 0.63	3.77 ± 0.55

As inorganic cores can be conveniently imaged with transmission electron microscopy (TEM), the mass of one NP core can be obtained. In addition to the NPs' core material density, the NP core volume Vc could be calculated using NP dimensions as obtained from TEM images (core diameter (dc)). Note, that without additional staining the organic shell does not provide contrast in regular TEM, thus only the inorganic cores are visible. In case of spheres the volume of one NP core is:

$$V_c(\text{sphere}) = \left(\frac{4\pi}{3}\right) \times \left(\frac{d_c}{2}\right)^3 = \left(\frac{\pi}{6}\right) \times {d_c}^3$$

In case the core is composed out of material of known density, the mass of one NP core is:

$$m_c = \rho_c \times V_c$$

For most inorganic NP materials their densities can be found in the literature. The molar mass of an NP core thus is:

$$M_c = m_c \times N_A$$

To give an example, for a spherical **NP2** with core diameter dc = $3.89 \cdot 10^{-7}$cm, Vc = (π/6) × $(3.71 \cdot 10^{-7}\text{cm})^3 = 3.08 \cdot 10^{-20}\text{cm}^3$. Given the bulk density of Au of ρ_{Au} = 19.3 g/cm^3, the mass of one Au core thus is $m_c = 19.3\ \text{g/cm}^3 \times 3.08 \cdot 10^{-20}\text{cm}^3 = 5.95 \cdot 10^{-19}$ g. The molar mass of an Au core thus is $M_c = m_c \times N_A = 5.17 \cdot 10^{-19}\ \text{g} \times 6.02 \cdot 10^{23}\ \text{mol}^{-1} = 3.58 \cdot 10^5$g/mol (Table 3.3). With these data and together with ICP-MS data analysis it is possible to calculate the concentration of gold NPs in a given solution (shown later, Table 3.4). These data are important for batch to batch reproducibility in the future encapsulation process.

Table3.3: NPs molecular weight as obtained from TEM diameter measurements.

	NP1	NP2	NP3	NP4	NP5
Mw (g/mol)	$6.54 \cdot 10^5$	$3.58 \cdot 10^5$	$2.91 \cdot 10^5$	$3.55 \cdot 10^5$	$3.26 \cdot 10^5$

UV/Vis absorption spectroscopy

UV/Vis absorption spectroscopy is an easy and simple method to characterize NPs. Spherical Au NPs of a few nm in size have their surface plasmon resonance (SPR) absorption peak around 510 nm[28] and do not absorb light at higher wavelengths of 800 - 1200 nm. We show in Figure 3.8 the UV-Vis spectra of **NP1-5** and the SPR wavelength values are summarized in Table 3.4.

[28]Woehrle, G.H.; Brown, L.O.; Hutchison, J.E. *J. AM. CHEM. SOC.* **2005**, 127, 2172-2183.

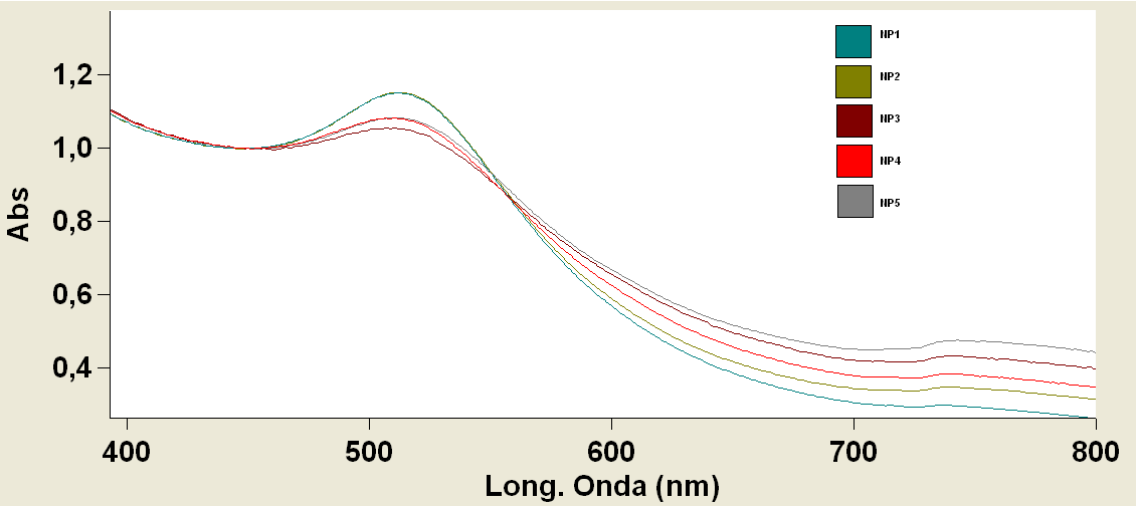

Figure 3.8: UV-Vis absorption of **NP1-5** normalized at λ = 450nm.

Table 3.4: Summary of NPs characterization parameters obtained by TEM, UV-Vis and ICP techniques.

	NP1	NP2	NP3	NP4	NP5
d_c(nm) ±σ	4.75 ± 0.66	3.89 ± 1.17	3.63 ± 0.49	3.88 ± 0.63	3.77 ± 0.55
$\lambda\ (nm, SPR)$	514	512	510	512	512
Concentration (μM)[a]	0.17	0.35	0.42	0.33	0.28

[a] *Calculated combining ICP-MS data and the Mw summarized in Table 3.3.*

The characteristic absorption peaks are responsible for the distinctive bright color of NP solutions. The spectral position and shape of the surface Plasmon absorption band depends on a variety of factors, such as NP material, size, size distribution, shape, surface chemistry, state of aggregation, as well as the solvent.[29] In our case, considering the gold core size of about 4 nm, SPR bands appear where expected in aqueous solution, that is, around 510 nm.

Due to the high batch to batch reproducibility in the synthesis of these types of gold NPs, concentration of the NPs solutions obtained in each synthesis was measured by UV-Vis after calibration of absorbance measured at λ = 450 nm using ICP-MS data of the first batch of each NP type (**NP1-5**). Hence, for every subsequent batch, absorption of each NP suspension is

[29]Huehn. J.; Carrillo-Carrion, C.;Soliman, M. G.; Pfeiffer, C.; Valdeperez, D.; Masood, A.; Chakraborty, I.; Zhu, L.; Gallego, M.; Yue, Z.; Carril, M.; Feliu, N.; Escudero, A.; Alkilany, A.; Pelaz, B.; del Pino, P.; Parak, W. J. J. Chem. Mater **2017**, 29, 399-461.

recorded, and then the NP concentration in this solution is determined by the calibration done with the help of ICP-MS data. (Annex I)

^{19}F NMR spectra of fluorinated NPs was also recorded to check the presence of a single and narrow fluorine signal, corresponding to the presence of 9 equivalent fluorine atoms in each ligand on **NP3-5** between -70 and -71 ppm, as shown in Figure 3.9.

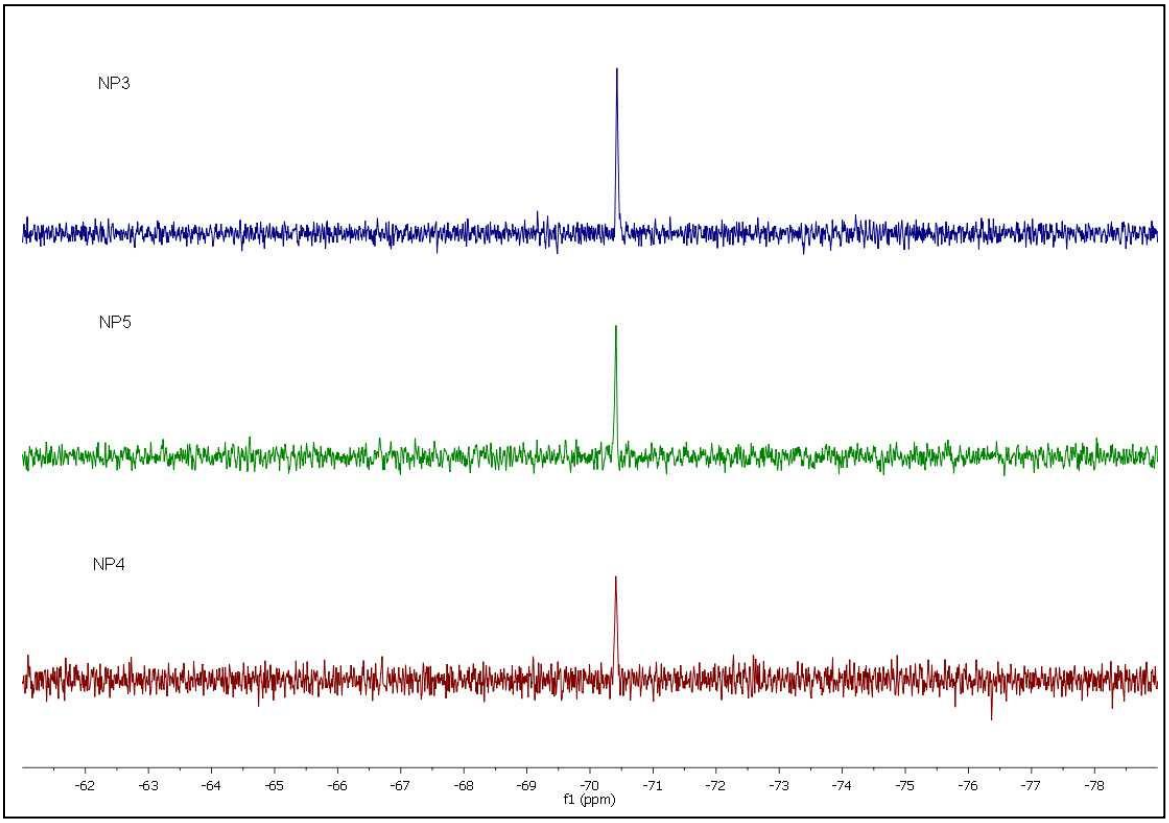

Figure 3.9: ^{19}F NMR spectra of **NP3** (top blue spectrum), **NP5** (medium green spectrum) and **NP4** (bottom red spectrum).

Once gold nanoparticles **NP1-5** were prepared and characterized, we moved to the next goal, that is, encapsulation of these NPs into gelatin nanoparticles, initially only with methoxylated **NP1-2** followed by **NP3-5** and evaluation of the ^{19}F NMR signal only for fluorinated ones.

3.3. Encapsulation of gold nanoparticles into gelatin nanosized spherical particles.

Two pathways of encapsulation have been tested, that is, passive encapsulation and covalent modification of gelatin chains.

3.3.1 Passive encapsulation by entrapment. (En-Gel).

Encapsulation by entrapment is obtained by simply adding simultaneously together gelatin and gold nanoparticles in solution. After the first desolvation step, then, by following exactly the same synthetic procedure as for regular gelatin NPs, we obtained gold NPs encapsulated in gelatin NPs by random entrapment of gold NPs during the second desolvation step followed by cross-linking, as described before.

Initially, we used gold nanoparticles **NP1** as surrogates because OMe group is non-charged. After initial successful trials with **NP1**, we attempted encapsulation with fluorinated **NP3**. The general synthetic strategy is depicted in Scheme 3.5.

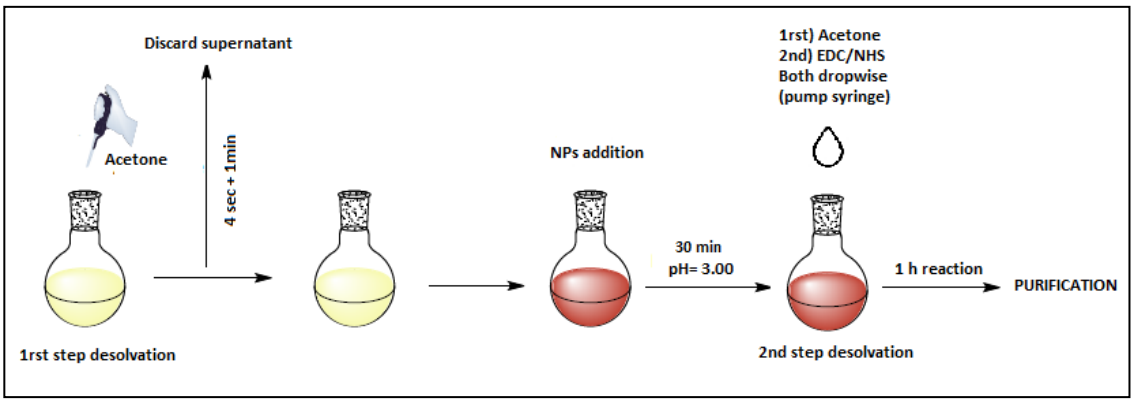

Scheme3.5: Schematic representation of the workflow used to prepare En-Gel containing either **NP1** or **NP3**.

Optimized parameters for En-Gel procedure:

- Temperature reaction: 50ºC
- Stirring: 750 rpm

- NPs addition after first desolvation step.
- pH = 3.00
- Acetone addition rate (2n desolvation step): 1 mL/min
- EDC/NHS ratio: 3.5:1 in a 0.9 % aqueous solution
- EDC/NHS addition rate: 0.1 mL/min
- 1 hour reaction time after EDC/NHS addition.

Unfortunately, the amount of NPs encapsulated by passive entrapment was very low, and most of the **NP1,3** were not incorporated into gelatin (showed up further, Table 3.9). Increasing the amount of NPs exposed to gelatin did not improve the encapsulation process for which En-Gel method was discarded, and a new method has been designedto increase encapsulation efficiency.

3.3.2 Gelatin covalent functionalization with AuNPs. (Au-Gel)

Molecules with reactive amino or carboxyl groups on gold nanoparticles may be coupled to proteins or modified polymeric supports using EDC and NHS as activators. Hence, following with this idea, we used our carboxylated NPs (**NP2**, **NP4** and **NP5**) to attach them to the gelatin chains before the 2nd desolvation step where gelatin NPs are formed, as it is shown in Scheme 3.6.

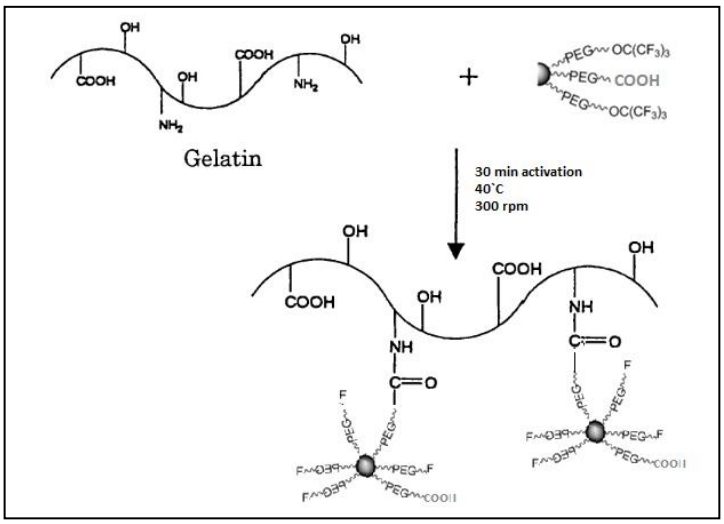

Scheme 3.6: Activation of gold nanoparticles and binding onto gelatin chains.

Being a completely new design not reported before, we did not know how many nanoparticles we would be able to attach without compromising the crosslinking of the gelatin nanoparticles, and hence an exhaustive optimization process was carried out.

For this strategy, this is how the procedure works: first activation of carboxyl groups on gold NPs by EDC/NHS takes place followed by immediate reaction with free amino groups on gelatin. Then, this gelatin chains modified with gold nanoparticlesis purified by centrifugation. The Au NP modified gelatin remains in the pellet and the supernatant are recovered fully transparent, which means that all gold nanoparticles have been bound to gelatin. The full procedure is shown in Scheme 3.7.

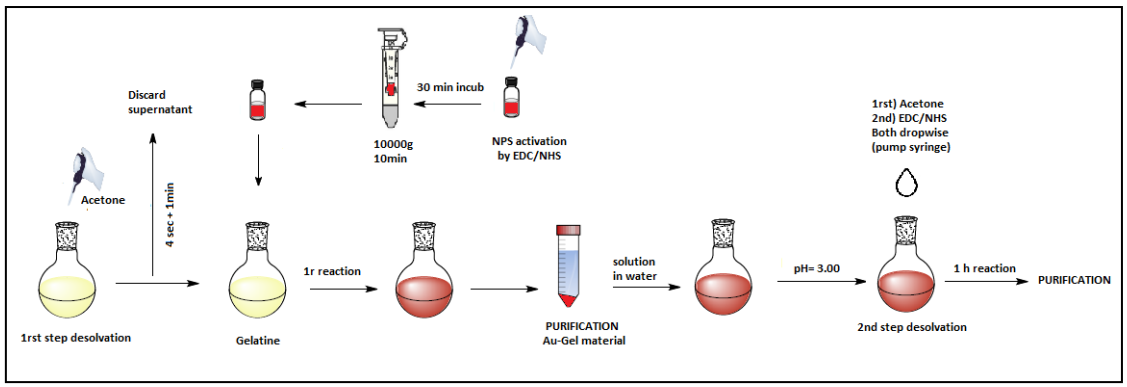

Scheme 3.7: Schematic representation of the workflow used to prepare Au-Gel containing **NP3**, **NP4** or **NP5**.

Next, this new material called Au-Gel (because there are already Au NPs attached to gelatin) was used to form gelatin NPs that already incorporate gold NPs. Hence, COOH groups from newly modified gelatin chains are subsequently activated also by EDC/NHS and reacted with the remaining free NH_2 groups from gelatin. This second amidation crosslinking step between functional groups both from the gelatin follows exactly the same conditions and parameters applied on unmodified gelatin chains.

From previous ICP-MS data collected for similar gold nanoparticles in our group,[10] it is estimated that there are approximately 140 ligands per nanoparticle, out of which 35 are funtionalized with carboxylic groups for **NP2**

and **NP4**, and 14 for **NP5**, due to the ligand ratios used in their respective syntheses. Therefore, at known concentration of **NP2,4-5**, we could estimate the concentration of carboxylic groups in solution and use this value to calculate EDC/NHS equivalents for each gold NP activation conditiontested. Hence, after optimization, the parameters for Au-Gel protocol are the following:

Activation of NPs conditions:

- Temperature: 40ºC
- Orbital stirring: 300 rpm
- Activation time: 30 min
- EDC/NHS ratio: 1:3

Covalent binding of activated Au NPs to gelatin chains:

- Temperature: 50ºC
- Stirring 750 rpm
- pH = 3.00
- NPs addition rate: 0.1mL/min
- 1 hour reaction time after Au NP addition.
- Non reacted Au NPs removal by centrifugation

Gelatin NPs formation with Au NP modified gelatin chains:

- Acetone addition rate (2n desolvation step): 1 mL/min
- EDC/NHS ratio: 3.5:1 in a 0.9 % aqueous solution.
- EDC/NHS addition rate: 0.1 mL/min
- 1 hour reaction time after EDC/NHS addition.

Increasing NPs quantities have been tried on this material in order to achieve the maximum loading of fluorinated Au NPs inside the gelatin nanoparticles as it will be shown in following sections.

As explained before, preliminary attempts were performed using methoxylated **NP2** and then we moved first to **NP4** and then to **NP5**. We are particularly interested in **NP5** because the ratio of fluorinated ligands is higher but there are still enough carboxylated ligands (10 %) to link to gelatin. All systems tested are summarized in Table 3.5.

Table 3.5: Sum up of the nanoparticles used in each encapsulation

	En-Gel1	En-Gel2	Au-Gel1	Au-Gel2	Au-Gel3
AuNPs contained	NP1	NP3	NP2	NP4	NP5

3.3.3. Purification

Unfortunately the present procedure to encapsulate nanoparticles does not synthesize a single size range of nanoparticles, thus, a purification process takes place in order to discard undesirable bigger sized nanoparticles. Both cases, En-Gel and Au-Gel were purified in the same way.

After crosslinking reaction at 50 ºC is over, the so-obtained suspension was transferred immediately into 50 mL centrifuge tube. The sample was centrifuged at 2000 g for 10 min, in order to separate nanoparticles of size ranging between 350 and 500 nm by DLS analysis. Pellet was collected and supertantant was centrifuged once more at 14000 g for 20 min. This time, obtained pellet is the desirable one, of size between 250-350 nm by DLS analysis. Supernanant was discarded (Scheme 3.8).

Pellets were resuspended in nano-H_2O, sometimes with the help of temperature or sonication to speed up the process. They can be safely stored at 4 ºC keeping colloidal properties overtime. Indeed, DLS of selected samples was measured after 2 months with no changes in size observed by DLS.

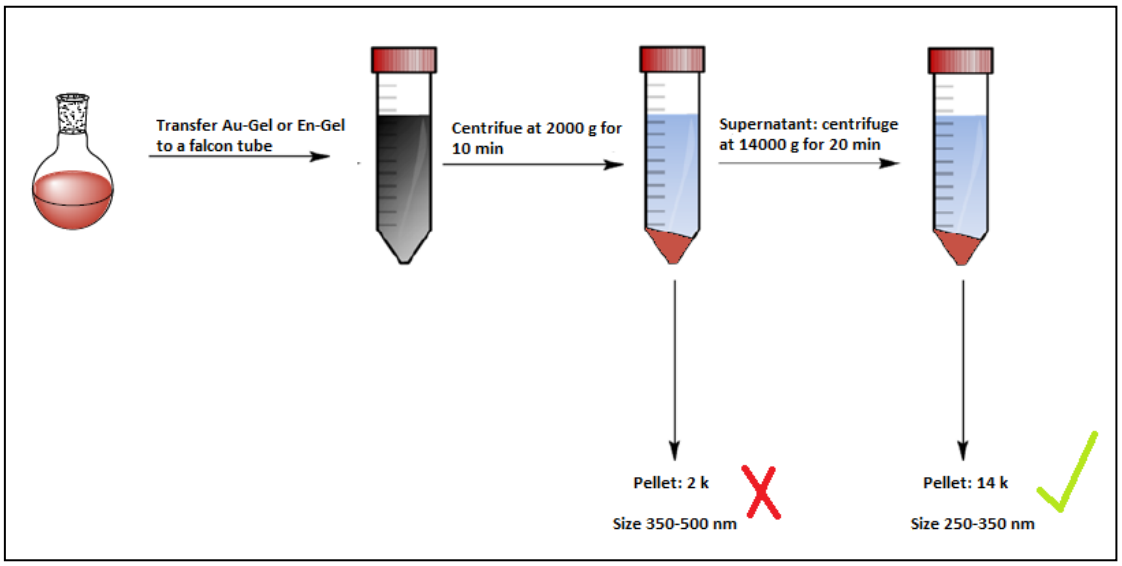

Scheme 3.8: Schematic representation of the workflow used to purify En-Gel and Au-Gel nanoparticles.

3.3.4 Caracterization of En-Gel and Au-Gel NPs

Dynamic light Scattering (DLS)

Dynamic light scattering is a simple and fast technique to measure hydrodynamic diameters of NPs and associated PdI. Solvent plays an essential role due to hydration/solvation, and also polymer architecture on the NPs in each solvent. In addition to measuring d_h average, it is possible to determine the monodispersity of NP suspensions by measuring polydispersity index (PdI). PdI is a unitless parameter that measures the heterogeneity in the NP's hydrodynamic diameter in sample. The DLS results obtained for En-Gel are summarized in Table 3.6, and those of Au-Gel are in Table 3.7.

Table 3.6:En-Gel encapsulation sphere's diameter displayed by Au NP/gelatin (μmol/mg) ratio employed in the synthesis.

NP/gelatin(10^{-6}μmol/mg)[a,b]		1.8	3.7	3.9	7.7
En-Gel1 (NP1)	d_h(nm)	262.2[c]	296.1 ± 51.3	×	×
	PdI	0.231[c]	0.312 ± 0.034	×	×
En-Gel2 (NP3)	d_h (nm)	×	×	332.0 ± 25	104.6[c]
	PdI	×	×	0.312 ± 0.037	0.178[c]

*[a]These values refer to the amount (μmol) of **NP1** or **NP3** added for encapsulation with respect to starting amount (mg) of gelatin. [b] 5.00 μL/mg gelatin of a 0.9 % of EDC:NHS (3.5:1) .[c]Experiment carried out only once.*

Table 3.7: Au-Gel encapsulation sphere's diameter displayed by Au NP/gelatin (μmol/mg) ratio employed in the synthesis.

NP/gelatin (10^{-6}μmol/mg)[a]		**1.4**[b]	[b]	[b]	[c]
Au-Gel1 (NP2)	d_h (nm)	289.8 ± 48.3			
	PdI	0.181 ± 0.06			
NP/gelatin (10^{-6}μmol/mg)[a]		**2.3**	**4.6**	**6**	**12**
Au-Gel2 (NP4)	d_h (nm)	355.0 ± 14.9	156.7[d]	267.1 ± 6.6	243.1[d]
	PdI	0.195 ± 0.03	0.655[b]	0.206 ± 0.04	0.154[d]
NP/gelatin (10^{-6}μmol/mg)[a]		**1.9**	**3.7**	**6.1**	**12**
Au-Gel3 (NP5)	d_h (nm)	297.3 ± 13.2	295.9[d]	289.1 ± 19.2	296.85 ± 14.5
	PdI	0.267 ± 0.12	0.244[d]	0.251 ± 0.06	0.149 ± 0.07

*[a]These values refer to the amount of **NP2**,**NP4** or **NP5** added for encapsulation with respect to starting amount (mg) of gelatin.[b] 5.00 μL/mg gelatin of a 0.9 % of EDC:NHS (3.5:1).[c] 2.67 μL/mg gelatin of a 0.9 % of EDC:NHS (3.5:1) .[d]Experiment carried out only once.*

Zetapotential

Zetapotential is the tool applied for calculating surface charge and the results for free gold nanoparticles (**NP1-5**), gelatin nanoparticles, En-Gel and Au-Gel encapsulated material are display on Table 3.8.

Table 3.8:Zetapotentialresults obtained in mV.

ZP (mV)	NP1	NP2	NP3	NP4	NP5	Empty gelatin NPs
Free AuNP[a]	-11.7	-8.7[b]	-15.0 ± 2.9	-17.2 ± 3.8	-16.0[b]	×
En-Gel	16.7[b,c,g]	×	21.7[b,d,g]	×	×	×
Au-Gel	×	18.6 ± 0.0[e,g]	×	20.3[b,f,h]	22.9 ± 3.9[f,h]	×
Gelatin	×	×	×	×	×	**18.4**[b]

*[a]Non encapsulated **NP1-5** were measured at a concentration of 0.01mM. [b]A single measurement was performed. [c]These nanoparticles were prepared using a ratio of 3.7 μmolNP per mg of gelatin. [d]These nanoparticles were prepared using a ratio of 3.9 μmolNP per mg of gelatin. [e]These nanoparticles were prepared using a ratio of 1.4 μmolNP per mg of gelatin. [f]These nanoparticles were prepared using a ratio of 6 μmolNP per mg of gelatin.[g] 5.00 μL/mg gelatin of a 0.9 % of EDC:NHS (3.5:1).[h] 2.67 μL/mg gelatin of a 0.9 % of EDC:NHS (3.5:1).*

As it is shown in Table 3.8 PEGylated gold nanoparticles surface is negatively charged. On the contrary, encapsulated nanoparticles following both pathways, that is, either by passive entrapment or by covalent bonding, show up positive values, thus, this is an indication that gold nanoparticles are mainly trapped inside gelatin and not linked or adsorbed on the surface of gelatin nanoparticles.

Inductively coupled plasma – mass spectrometry (ICP-MS)

With inductively coupled plasma coupled with mass spectrometry (ICP-MS) quantitative elemental analysis of gold can be performed.

Table 3.9: Encapsulation Efficiency calculated based on initial **NP1-5** concentration added in reaction vs. final quantity of Au in sample measured by ICP.

	Au $NP_{initial}$(10^{-3}µmol)	Au by ICP$(\mu g/L)$[a]	Au NP_{final}(10^{-4}µmol)	Au NP/gelatin (10^{-6}µmol/mg)[b]	EE (%)
En-Gel1 (NP1)[c]	0.268	10.06	0.014	0.24	**0.52**
En-Gel2 (NP3)[d]	0.579	29.57	0.061	0.71	**1.05**
Au-Gel1 (NP2)	0.210[e]	55.06	0.138	0.62	**6.59**
	0.420[f]	254.23	1.060	2.46	**25.35**
Au-Gel2 (NP4)	0.215[f]	255.52	0.755	3.15	**35.19**
	1.800[g]	944.21	3.980	22.10	**22.16**
Au-Gel3 (NP5)	0.890[h]	248.31	0.937	6.53	**10.45**
	1.800[g]	437.24	1.690	5.09	**9.40**

[a]Data obtained for 6 mL of digested sample .[b]Amount of Au NP (µmol) per mg of Au-Gel NPs of the final product.[c]Starting from $3.7{\cdot}10^{-6}$µmolNP per mg of gelatin.[d]Starting from $3.9{\cdot}10^{-6}$µmolNP per mg of gelatin. [e]Starting from $0.7{\cdot}10^{-6}$µmolNPper mg ofgelatin.[f] Starting from $1.4{\cdot}10^{-6}$µmolNP per mg of gelatin. [g]Starting from $1.2{\cdot}10^{-6}$µmolNP per mg of gelatin. [h]Starting from $6.0{\cdot}10^{-6}$µmolNP per mg of gelatin.

$$EE = 100 - \frac{(initial\ mols\ NP - final\ mols\ NP)}{initial\ mols\ NP} \cdot 100$$

It has to be mentioned that encapsulation efficiency (EE) reflects only the amount of starting Au NPs that are incorporated in the final Au-Gel NPs, regardless of the amount or Au NPs pernanoparticle of gelatin. Indeed, through purification process, a second population of Au-Gel nanoparticles encapsulated is discarded due to their bigger size because the synthetic pathway applied on Au-Gel encapsulation does not offer a single homogeneous particle size. Hence, encapsulation efficiency percentages displayed in Table 3.9 are only those of nanoparticles under suitable diameter size range. However, what is more important for us is the amount of Au NPs inside each gelatin NP which was been reflected in Table 3.9 as the ratio of AuNPs (µmol) per mg of final gelatin NP, which is highest for Au-Gel2 with a value of $22.1{\cdot}10^{-6}$ µmol/mg.

Since we discarded En-Gel procedure due to low efficiency encapsulation we continued with further characterization of Au-Gel encapsulation as a very promising system.

Transmission electron microscopy (TEM)

ZP in combination with TEM is a way to prove Au NPs are mostly encapsulated inside the gelatin nanospheres. TEM microscopy has been carried out in order to support these results and no free unattached gold NPs outside the gelatin ones have been detected at all in any TEM micrograph so far. This fact, together with no changes observed in ZP seems to confirm that gold NPs are actually encapsulated.

In the following Figures we show selected TEM micrographs and size data for different Au-Gel NPs performed under negative staining.

Au-Gel 1	
NP2/gelatin (10^{-6}µmol/mg)[a]	1.4
d (nm) by TEM	217.0 ± 62.8

[a]*Amount of **NP2** added for encapsulation with respect to starting amount (mg) of gelatin.*

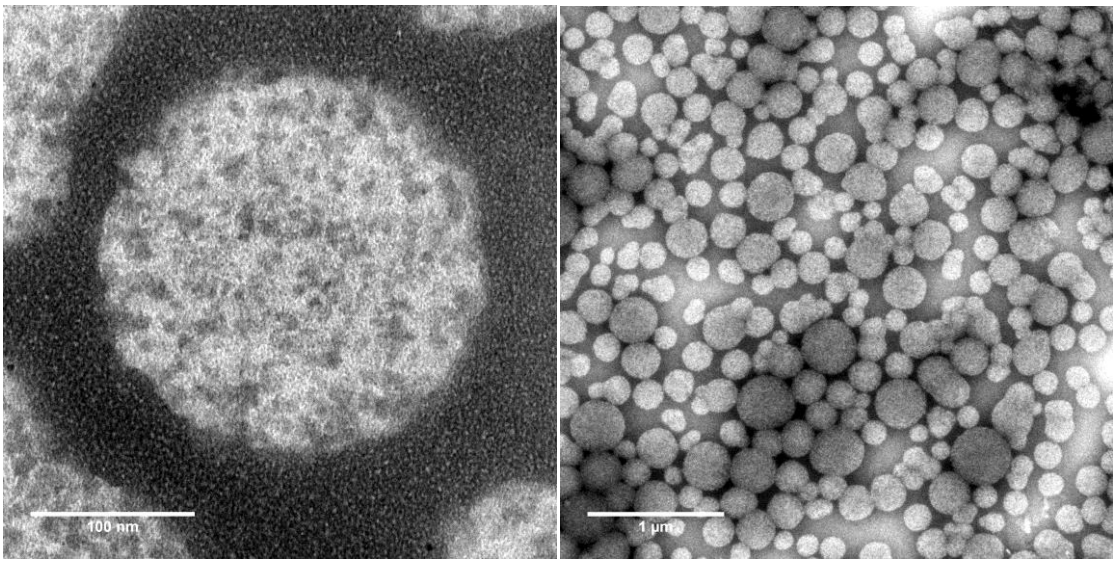

Au-Gel 2	
NP4/gelatin (10^{-6}µmol/mg)[a]	4.60
d (nm) by TEM	218.9 ± 52.1

[a]*Amount of **NP4** added for encapsulation with respect to starting amount (mg) of gelatin.*

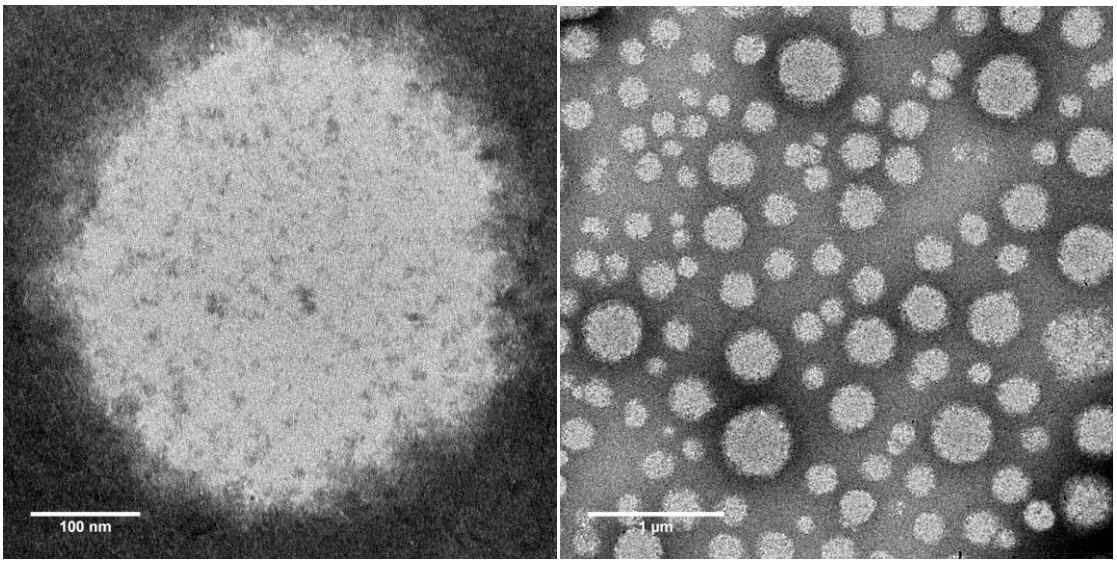

Au-Gel 3	
NP5/gelatin (10^{-6}µmol/mg)[a]	12.00
d (nm) by TEM	206.9 ± 59.3

[a]*Amount of **NP5** added for encapsulation with respect to starting amount (mg) of gelatin.*

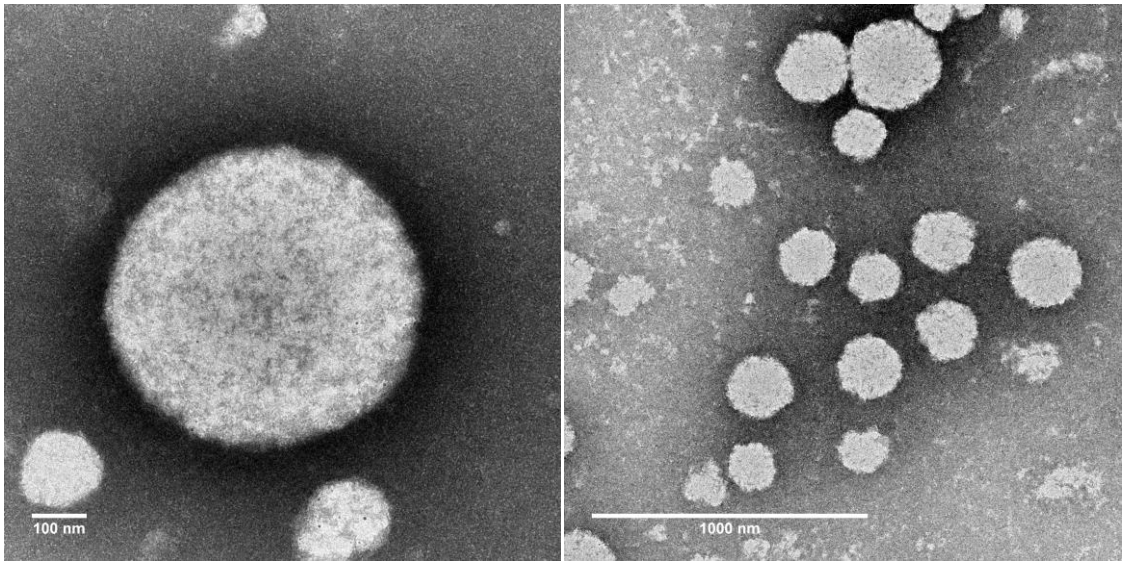

Figure 3.10: TEM micrographs at different magnifications of Au-Gel1, Au-Gel2 and Au-Gel3.

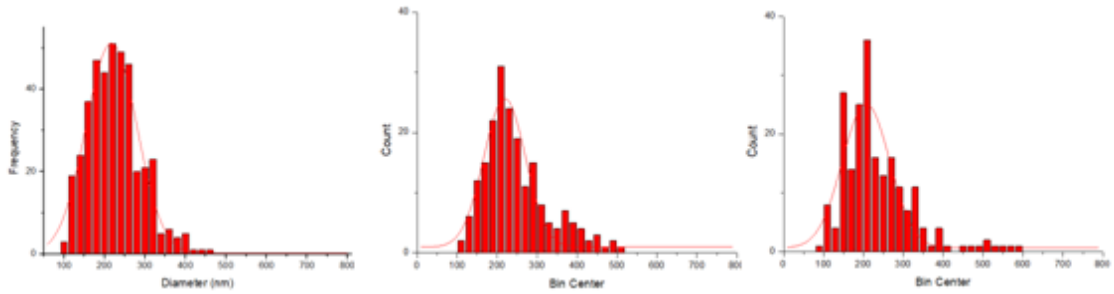

Figure 3.11: Histograms with Gaussian distribution size of Au-Gel1, Au-Gel2 and Au-Gel3 (from left to right) calculated by Origin 8.5 software.

As we can see on Figure 3.10 (plus statistics on Figure 3.11), there are no aggregates, particles are quite homogeneous, but still purificationcan be optimized. What TEM negative stain shows up is organic material, ergo, brightened contrast is gelatin.

At this stage an important issue came up. Gelatin nanoparticles are soluble in water, also are gold nanoparticles. With first reaction conditions using 1.4 - $4.6 \cdot 10^{-6}$ µmol of Au NPs per mg of gelatin we did not encounter problems at all when resuspending final AuGel nanoparticles pellets after purification. Unfortunately increasing ratios to 6 and $12 \cdot 10^{-6}$ µmol **NP5** per mg gelatin we could not resuspend pellets easily in aqueous media, even applying heat and sonication. So we decided to revisit the crosslinking conditions used for these gelatin NPs preparation and we evaluated the use of less crosslinker to increase solubility of gelatin NPs.

Indeed, less EDC/NHS quantity allows to resuspend Au-Gel nanoparticles successfully in water. We decided to reduce the amount of 0.9 % EDC/NHS (3.5:1) solution added to the reaction. Hence, we moved from initially optimized 5 µL/mg of gelatin to 3.33 µL/mg and to 2.67 µL/mg (Table 3.10). In this manner, the rigidity of the gelatin NPs is reduced, hydration is favored, more free amino groups are available in gelatin after crosslinking and solubility is overall enhanced.

Table 3.10: Au-Gel encapsulation sphere's diameter displayed by different crosslinker quantity.

EDC/NHS solution per gelatin (µL/mg)		5.00	3.33	2.67
Au-Gel 2 (2.30)[a]	d_h (nm)	354.4[b]	355.0 ± 14.9	288.5[b]
	PdI	0.187[b]	0.199 ± 0.042	0.264[b]
Au-Gel 3 (5.99)[a]	d_h (nm)	297.3 ± 13.2	×	257.9 ± 39.2
	PdI	0.267 ± 0.12	×	0.271 ± 0.12

[a]*The value in brackets refers to the amount of **NP4** or **NP5** added for encapsulation with respect to starting amount (mg) of gelatin .*[b]*A single measurement was performed*

Lastly, another issue was sorted out.In the initial experiments, after 1 hour reaction between gelatin and EDC/NHS activated **NP5**, red color was observed in the supernatant which meant that the covalent linkage between **NP5** and gelatin chains was not achieved quantitatively (free nanoparticles remained in supernatant). We thought that several carboxyl groups either remained inactive due to accessibility problems and steric hindrance on the NP surface or were being hydrolized. Thus, the amount for EDC/NHS for the activation of gold nanoparticles was increased for **NP5** from 56 to 100 equivalents of EDC**,** until the recovered supernatants were clear and without NPs in solution, meaning no NPs were recovered unattached after conjugation with gelatin.

Nuclear Magnetic Resonance (NMR)

Lastly, but mainly the top goal of the present work, we wanted to check if we could modulate the ^{19}F NMR signal of the fluorinated gold NPs by encapsulation in gelatin, as the OFF state of our potential OFF/ON probe.

Fluorine labeled gold nanoparticles display a single intense ^{19}F NMR and ^{19}F MRI signal as already demonstrated.[10] Besides, encapsulation of those particles was never tested before. For this reason, ^{19}F NMR spectrum has been analyzed in order to check if gelatin encapsulation is able to quench fluorine signal from gold nanoparticles, as we hypothesized and as the first step towards our OFF/ON probe.

^{19}F NMR spectra of non-encapsulated nanoparticles **NP4** and Au-Gel nanoparticles where **NP4** was encapsulated at equivalent gold NP concentration as calculated from ICP-MS analysis, were measured and the signal obtained was compared.

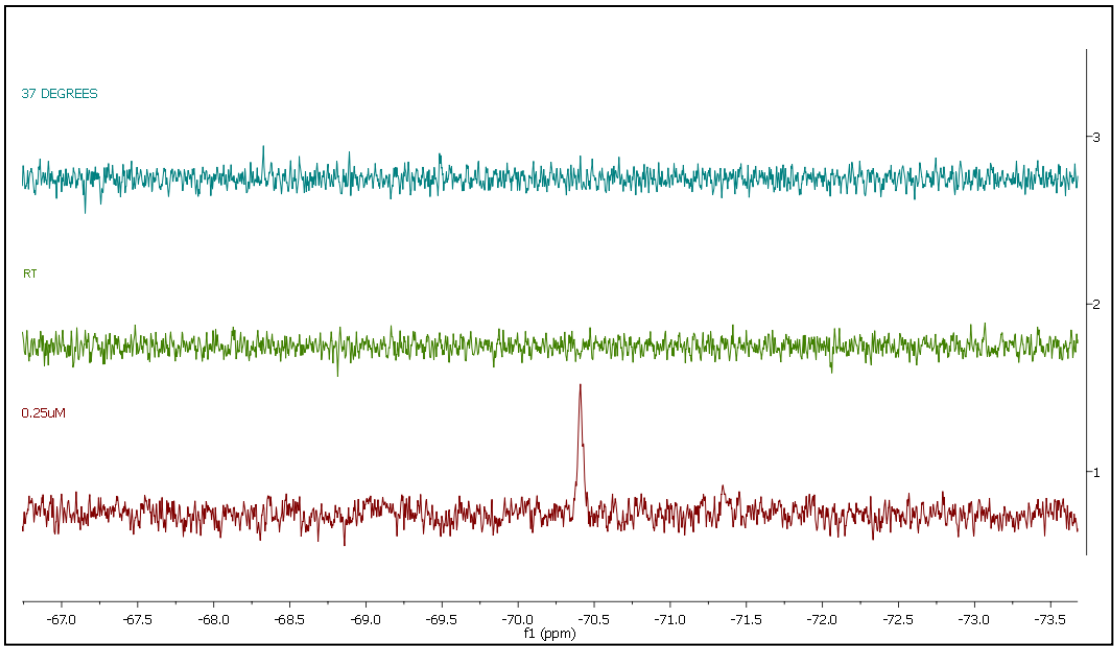

Figure 3.12: ^{19}F NMR of **NP4** and Au-Gel2 encapsulated nanoparticles. Red spectrum corresponds to non-encapsulated **NP4** at known concentration (0.25 μM), blue and green spectra correspond to Au-Gel2 at equivalent Au NP concentration at 37 and 25 ºC, respectively.

As it can be observed in Figure 3.12 we successfully quenched ^{19}F NMR signal through gelatin encapsulation both at room temperature (25 ºC) and at physiological temperature (37ºC). Last NMR spectrum shows ^{19}F NMR of free nanoparticles at same concentration than encapsulated ones showing the characteristic peak for fluorine in these NPs, for comparison.

Next, activation of the signal in the presence of MMP-9 is to be tested in the future, although this is beyond the time frame of this work.

4. Conclusion

A new material has been designed with potential OFF/ON features with application in ^{19}F magnetic resonance. Initially, passive trapping of gold nanoparticles was the goal but it was discarded due to low efficiency in encapsulation. The significant scientific advance is based on the covalent functionalization of gelatin chains with partially carboxylated and fluorinated gold nanoparticles.

In the present work it has been proved that gold nanoparticles remain inside the gelatin sphere via two step desolvation method of encapsulation. NMR has demonstrated that gelatin encapsulation quenches fluorine signal successfully, thus, OFF state as the initial point of an activatable probe has been proved.

Furthermore, it has to be mentioned that this process can be scaled up due to its simplicity. It is a non toxic procedure, ergo safe. This new material based on gelatin chain modification ensures high efficiency in encapsulation without losing gold nanoparticles making our system much more competent.

5. Materials and Methods

5.1. Gelatin Nanoparticles synthesis

General considerations:

Gelatin type A and NHS were purchased from Sigma Aldrich and EDC from Fluka Analytical. Solvents (analysis quality) were purchased from Panreac and used as received. Water is MilliQ quality. A Sigma bench centrifuge was used for centrifugations. For reagent addition a WPI SP210IWZ syringe pumpwas used.

Typical procedure:

First step desolvation: The hot plate was set to 50 ºC and we waited until the temperature was stable. 300 mg of gelatin type A was weighted and placed in a 50 mL round bottom flask with a stirrer. 6 mL of nanopure-H_2O was added, carefully without splashing the flask's walls. The round bottom flask was put to heat stirring at 1000 rpm. After 10 min until complete dissolution was waited and then stirring was fixed to 750 rpm.

6 mL acetone was added at once to the vortex of the solution smoothly with a syringe. Then we waited 4 seconds, removed the flask from the hot plate and high molecular weight gelatin precipitated during exactly 1 minute. The supernatant was poured out from the round bottom flask.

Again 6 mL nano-H_2O was added on the precipitate. The round bottom flask was put to heat with stirring at 1000 rpm and we leaved mixing for 10 min until complete dissolution. Then, the round bottom flask was took out and let it reach room temperature. pH of the solution was measured and adjusted carefully to 3.00 sharp by adding 1M HCl.

Second step desolvation: The round bottom flask was taken back to the hot plate to 50 ºC and 750 rpm and we waited for 5 min in order to ensure it reached the desirable stirring rate and temperature. With a syringe pump was added 19.92 mL acetone at 1 mL/min rate to solution's vortex (keeping 750 rpm

and 50 ºC conditions until reaction was over). After the addition of approximately 8 mL of acetone the reaction began to turn turbid.

Subsequently, also with a syringe pump, freshly prepared 0.9 %EDC/NHS (3.5:1) solution was added according to the desirable crosslinkage amount (5.00 µL/mg of starting gelatin ratio. EDC/NHS solution was added at 0.1 mL/min rate. The flask was covered and left reacting for 1h.

Purification: After 1 hour, the crude reaction was transferred to two 10 mL centrifuge falcons. They were centrifuged at 2000 g once for 15 min at RT in SIGMA centrifuge. Resulting pellets (nanoparticles diameter between 500-350 nm) were resuspend in 3 mL nano-pure water for further DLS characterization and stored.

Supernatants were transferred in a new 10 mL falcon tube and centrifuged at 14000 g once for 20 min. The resulting pellets (nanoparticles diameter between 350-250 nm) were resuspended in 3 mL H_2O nano-pure water for further DLS characterization and stored. Some pellets needed sonication and/or be heated to achieve successfully and homogeneous solution.

Storage: Resulting samples were stored at 4 ºC to ensure long time colloidal stability.

5.2. Gold nanoparticles synthesis

General considerations:

$HAuCl_4$ was purchased from Strem Chemicals and $NaBH_4$ from Sigma Aldrich. Solvents (analysis quality) were purchased from Panreac and used as received. Water is MilliQ quality. A Beckmann Coulter J-26XP floor ultracentrifuge was used for ultracentrifugations. Samples were introduced in 4 mL Beckman centrifuge tubes.

PEGylated ligands HS-PEG-OMe (2kDa) and HS-PEG-COOH (3kDa) were purchased from Rapp Polymere. Fluorinated PEG ligand HS-PEG-F (3 kDa) was prepared in the laboratory as described by us (Scheme 3.3).[10]

General procedure:

Synthesis: The corresponding PEGylated ligand (see Table 3.1) dissolved in CH_2Cl_2 (0.45 equiv.) were added under stirring onto CH_2Cl_2 (8 mL/µmol of $HAuCl_4$).

Subsequently, a solution of $NaBH_4$ (0.1 M, 5 equiv.) was freshly prepared in ice-cold methanol, besides a solution of $HAuCl_4$ (25 mM, 1 equiv.) in ice-cold methanol was added to the reaction mixture. One minute after the preparation of $NaBH_4$ solution, the latter was added dropwise to the ligand/gold mixture already in the flask. When last $NaBH_4$ drop was in solution reaction was stirred for 30 seconds. Afterwards, the resulting red solutiton was allowed to stand for at least 12 hours without stirring and capped to avoid solvent evaporation.

Purification: After 12 hours, solvent was evaporated in the rotary evaporator and the so-obtained NPs were purified by ultracentrifugation. First, 2 cycles of 2 hours at 150000 g were used to remove free unbound ligands and salts in the supernatant, and then 2 cycles of 30 minutes at 50000 g were used to discard aggregates and too big nanoparticles in the pellet. Hence **NP1-5** were recovered in the supernatant after 50000 g centrifugation as depicted in Figure 5.1.[10]

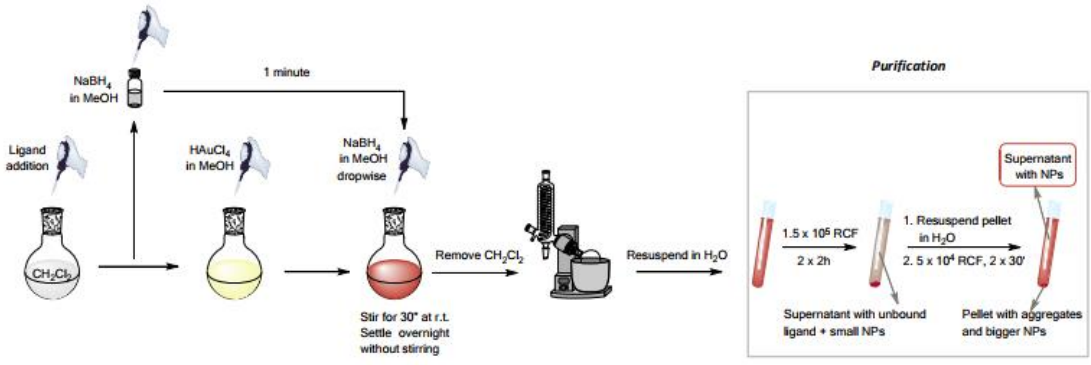

Figure 5.1: Schematic representation of the workflow used to synthesize and purify gold nanoparticles.

5.3. Preparation of gelatin nanoparticles by passive encapsulation.

Typical procedure:

First step desolvation: The hot plate was set to 50ºC and waited until the temperature was stable. 300 mg of gelatin type A was weighted and placed in a 50 mL round bottom flask with a stirrer. 6 mL nanopure-H_2O was added, carefully without splashing the flask's walls. The round bottom flask was put to heat stirring at 1000 rpm. We waited 10 min until complete dissolution and then fixed the stirring to 750 rpm.

At once 6 mL acetone was added to the vortex of the solution smoothly with a syringe. Then after 4 seconds, the flask was removed from the hot plate and let high molecular weight gelatin precipitate for exactly 1 minute. The supernatant was poured out from the round bottom flask.

Nanoparticles addition: Nanoparticles **NP1** or **NP3** prepared on section 5.2. were added at known concentration onto the gelatin after first desolvation and water was added until the final volume was 6 mL. Solution was stirring for 10 min at 50 ºC. Then, we took out the round bottom flask and leave it reach room temperature. pH of the solution was measured and adjusted carefully to 3.00 sharp by adding 1M HCl.

Second step desolvation: The round bottom flask was took back to the hot plate at 50ºC and 750 rpm and stirred for 30 min in order to ensure homogeneity. With a syringe pump 19.92 mL acetone was added at 1 mL/min rate to solution's vortex (keeping 750 rpm and 50ºC conditions until reaction was over). After the addition of approximately 8 mL of acetone the reaction began to turn turbid.

Subsequently, also with a syringe pump, freshly prepared 0.9 % EDC/NHS (3.5:1) solution was added according to the desirable crosslinkage amount (5.00 µL/mg of starting gelatin ratios). EDC/NHS solution was added at 0.1 mL/min rate. The flask was covered and left reacting for 1h.

Purification: After 1 hour, the crude reaction was transfered to two 10 mL centrifuge falcons. They were centrifuged at 2000 g once for 15 min at RT in the SIGMA centrifuge. Resulting pellets (nanoparticles diameter between 500-350 nm) were resuspened in 3 mL nano-pure water for further DLS characterization and stored.

Supernatants were transferred in a new 10 mL falcon tube and centrifuged at 14000 g once for 20 min. The resulting pellets (nanoparticles diameter between 350-250 nm) were resuspended in 3 mL H_2O nano-pure water for further DLS characterization and stored. Some pellets needed sonication and/or be heated to achieve successfully and homogeneous solution.

Storage: Resulting samples were stored at 4 ºC to ensure long time colloidal stability.

5.4. Preparation of Au-gelatin nanoparticles by covalent functionalization

General procedure:

Nanoparticles activation of carboxyl groups: Gold nanoparticles already prepared in section 5.2. **NP2,4-5** at known concentration and selected amount (see Tables 3.7 and 3.9 for each condition tested) were transferred to avial for activation reaction.

From previous ICP-MS data collected for similar gold nanoparticles in our group, it was estimated that there are approximately 140 ligands per nanoparticle, out of which 35 ligands are functionalized with COOH for **NP2** and **NP4**, and 14 ligands for **NP5**. Therefore, at known concentration of **NP2,4-5**, we could estimate the concentration of COOH groups in solution (1 equiv.).

For **NP2** and **NP4,** the optimized NHS/EDC amounts were 85 equiv. NHS (5µM in water) followed by 249 equiv. EDC (5µM in water). For **NP5** the optimized NHS/EDC amounts were 100 equiv. NHS (5 µM in water) followed by 300 equiv. EDC (5 µM in water).

The reaction vial was heated at 40 ºC under orbital stirring at 300 rpm for 30 min. Then, the activated AuNPs solution were filtered by centrifugation (Amicon filters 100 kDa MWCO) in order to remove non reacted EDC/NHS. Hence, the sample was centrifuged at 3500 g twice for 2 min at RT in the SIGMA centrifuge. Resulting purified nanoparticles were diluted to a fixed volume of 1.5 mL nano-pure water.

First step desolvation: The hot plate was set to 50ºC and waited until the temperature was stable. 300 mg of gelatin type A were weighted and placed in a 50 mL round bottom flask with a stirrer. 6 mL nanopure-H_2O was added, carefully without splashing the flask's walls. The round bottom flask was put to heat stirring at 1000 rpm. We waited for 10 min until complete dissolution and then fixed the stirring to 750 rpm.

At once 6 mL of acetone was added to the vortex of the solution smoothly with a syringe. Then after 4 seconds, the flask was removed from the hot plate and let high molecular weight gelatin precipitate for exactly 1 minute. The supernatant was poured out from the round bottom flask.

Again 6 mL nano-H_2O was addedon the precipitate. The round bottom flask was put to heat with stirring at 1000 rpm and mixed for 10 min until complete dissolution.

This first desolvation step must be done before or in parallel to Au NPs activation to avoid Au NPs deactivation over time.

Nanoparticles addition: with a syringe pump, the purified activated nanoparticles resuspended in 1.5 mL solution were added onto 6 mL gelatin solution at 0.1 mL/min speed (keeping 750 rpm and 50ºC reaction conditions). The mixture was allowed to react for 1 h.

Au-Gel material purification: Onto resulting solution, we added at once 21 mL of acetone into the round bottom flask in order to precipitate gelatin chains modified with Au NPs (still at 750 rpm and 50 ºC reaction conditions).

Then the solution was transferred to two 10 mL centrifuge falcon tubes and centrifuged once at 10000 g for 10 min at RT in the SIGMA centrifuge to remove unreacted gold nanoparticles.

The so obtained pink gelatin pellet was transferred back into a round bottom flask. 6 mL nano-H_2O was addedand heated at 50 ºC with 1000 rpm stirring for 10 min until complete dissolution of the gelatin pellet.

Then, the round bottom flask was taken out from heat and stirring and leave it reach room temperature.pH of the solution was measured and adjusted carefully to 3.00 sharp by adding 1M HCl.

Second step desolvation: The round bottom flask was taken to the hot plate to 50 ºC and 750 rpm and wait for 5 min in order to ensure it reaches the desirable stirring rate and temperature. With a syringe pump 19.92 mL acetone was added at 1 mL/min rate to solution's vortex (keeping 750 rpm and 50ºC conditions until reaction was over). After the addition of approximately 8 mL of acetone the reaction began to turn turbid.

Subsequently, also with a syringe pump, freshly prepared 0.9 % EDC/NHS (3.5:1) solution was added according to the desirable crosslinkage amount (Table 3.10 being 5.00 / 3.33 / 2.67 µL/mg of starting gelatin ratios). EDC/NHS solution was added at 0.1 mL/min rate. The flask was covered and left reacting for 1h.

Purification: After 1 hour, the crude reaction was transferred to two 10 mL centrifuge falcons. They were centrifuged at 2000 g once 15 min at RT in the SIGMA centrifuge. Resulting pellets (nanoparticles diameter between 500-350 nm) were resuspended in 3 mL nano-pure water for further DLS characterization and stored.

Supernatants were transferred in a new 10 mL falcon tube and centrifuged at 14000 g once for 20 min. The resulting pellets (nanoparticles diameter between 350-250 nm) were resuspended in 3 mL H_2O nano-pure water for further DLS characterization and stored. Some pellets needed sonication and/or be heated to achieve successfully and homogeneous solution.

Storage: Resulting samples were stored at 4 ºC to ensure long time colloidal stability.

5.5. Characterisation techniques

5.5.1. Dynamic light scattering (DLS)

DLS experiments are based on the Brownian motion of the analyts within the dispersion medium is detected. More specifically, this is done by measuring the angular distribution of time/dependent scattered light intensity due to density and/or concentration fluctuations.[30] This fluctuations give information of diffusion coefficient of the analyts sample. Thus, diffusion coefficient in turn represents the analyt's Brownian motion. Finally, size is calculated based on measured velocity respect physic factors such viscosity and temperature.

Hydrodinamic diameter (d(H)) can be calculated by Stokes-Einstein equation:

$$d(H) = \frac{kT}{3\pi\eta D}$$

d(H)	=	hydrodynamic diameter
k	=	Bolzmann's constant
η	=	viscosity
T	=	absolute temperature (K)
D	=	diffusion coefficient

Thereby, the measured diameter (d(H)) describes how the particles move within a liquid, thus, cannot be understand equivalent with the actual particle diameter.

DLS displays average size, also polydispersity index (PI) giving information about the actual distortion of the monomodal light scattering signal.

[30] Static and dynamic light scattering from branched polymers and biopolymers, Ed. Springer-Verlag. Berlin 1983.

The PI have values from 0-1 and, being 0 an ideal homogenous system and 1 non homogenous distribution.

DLS experiments were performed with Zetasizer (Nano ZS ZEN3600) detecting the scattered light at a fixed angle of 175º. Viscosity parameter was set up as pure water (i.e. 08872 cP at 25ºC). The experiments were performed at room temperature settled to 25 ºC in Zetasizer.

5.5.2. Inductively coupled plasma-mass spectrometry (ICP-MS)

Quantitative elemental analysis of gold can be performed by inductively coupled plasma coupled with mass spectrometry (ICP-MS). Dilution and acid digestion are required prior to analysis. For the case of our gold NP loaded gelatin NPs, 0.2 mL of gelatin NPs solution were firstly lyophilized and then digested with 1 mL of aqua regia (i.e. concentrated HCl (35 wt%) and HNO_3 (67 wt%) in 3:1 molar ratio) and then left overnight to allow oxidation of metallic cores into their corresponding ions. On next morning, 5 mL of HCl (2 %) were added before ICP-MS analysis.

5.5.3. Transmission electron microscopy (TEM)

All nanoparticles were analyzed by TEM to characterize the morphology of dry nanoparticles. The pictures were taken with a field transmission scanning electron microscope JEOL JEM-2100F working at 200 kV.

Sampling preparation: by deposition of the sample (highly diluted) on top of a copper grid coated with a layer of carbon for standard TEM. For negative staining uranyl acetate was employed as the staining solution. In this manner, the background is stained, leaving the particle untouched, and thus visible.

Size measurement was performed with free ImageJ software and size distribution analysis and histogram production was done with Origin® software.

Selected TEM figures are displayed in Figures 3.4, 3.7 and 3.10 in section 3.

5.5.4. Zetapotential (ζ) determination

As the z potential cannot be measured directly, it is calculated from the electrophoretic mobility of an analyte, according to the Debey-Huckel-theory and the Helmholtz-Smoluchowski-equation.

For the present study, we used a Zetasizer (Nano ZS ZEN3600). Measurements were performed in specific disposable cuvettes in water media (conductivity: $5.5 \cdot 10^{-6}$ S/m).

Zeta potentials values are displayed in Table 3.8 in section 3.

5.5.5. Ultraviolet Visible Spectroscopy (UV-Vis)

UV-Vis absorption spectra were measured in a spectrophotometer UV-Vis-NIR Cary 5000 Varian. Normalized at λ = 450 nm.

UV-Vis spectra are displayed in Figure 3.8 in section 3.

In the case of fluorinated **NP3-5**, NP concentration for new batches was calculated by UV-Vis and ICP-MS calibration with the first batch of each NP. Hence, initially, increasing concentrations of gold NPs calculated by ICP were measured in UV-Vis and the absorbance at λ = 450 nm was plotted against concentration of NPs (μM). The so-obtained calibration graphs for **NP3-5** are plotted in the Annex I.

5.5.6. Nuclear Magnetic Resonance (NMR)

^{19}F NMR spectra were measured in a Bruker AVANCE (500MHz). Samples were carried out in water with a 20% of D_2O.

NMR spectra are displayed in Figures 3.9 and 3.12 in section 3.

Annex I

1. Calibration of NP3, NP4 and NP5.

Calibration line was plotted concentration (µM) from ICP-MS data first batch of each NPs synthesized vs. absorbance.

NP3: 100% HS-PEG- F

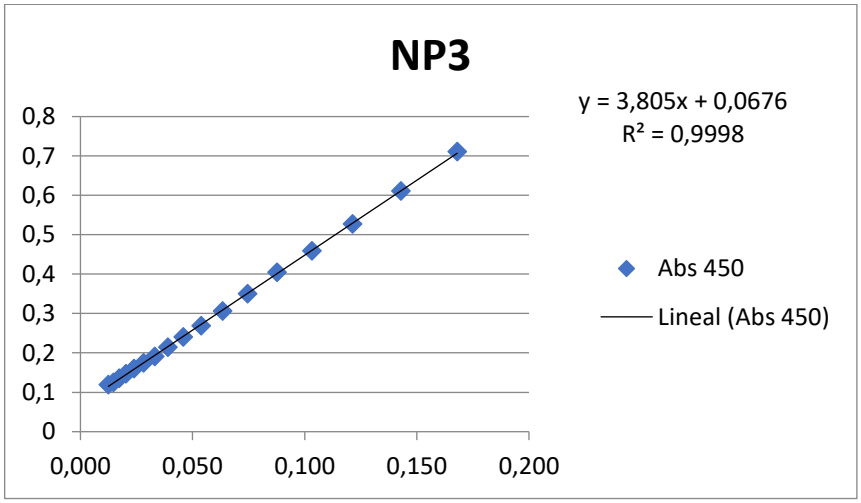

Graph A: Calibration line of **NP3**.

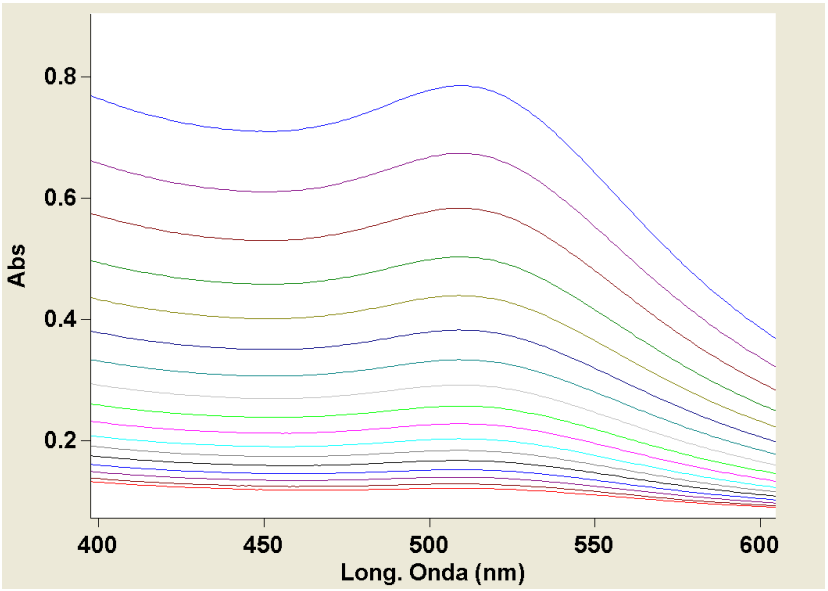

Figure A: UV-Vis absorption of **NP3** at different concentrations.

NP4: 75% HS-PEG-F and 25% HS-PEG-COOH

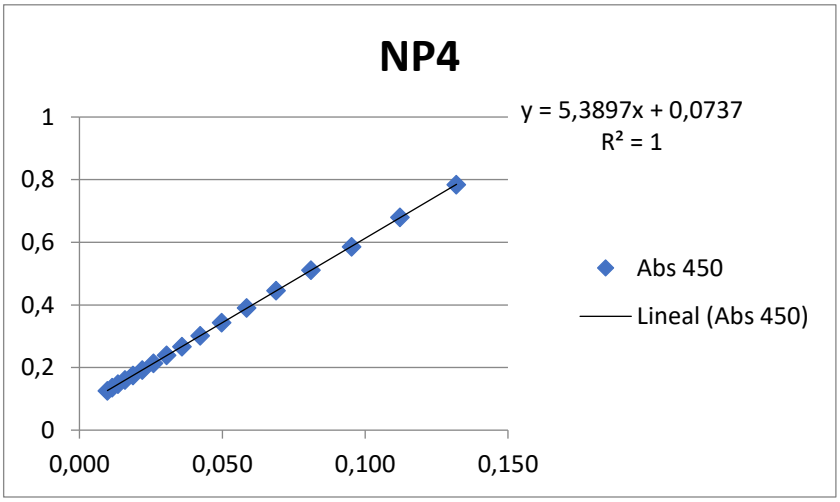

Graph B: Calibration line of **NP4**.

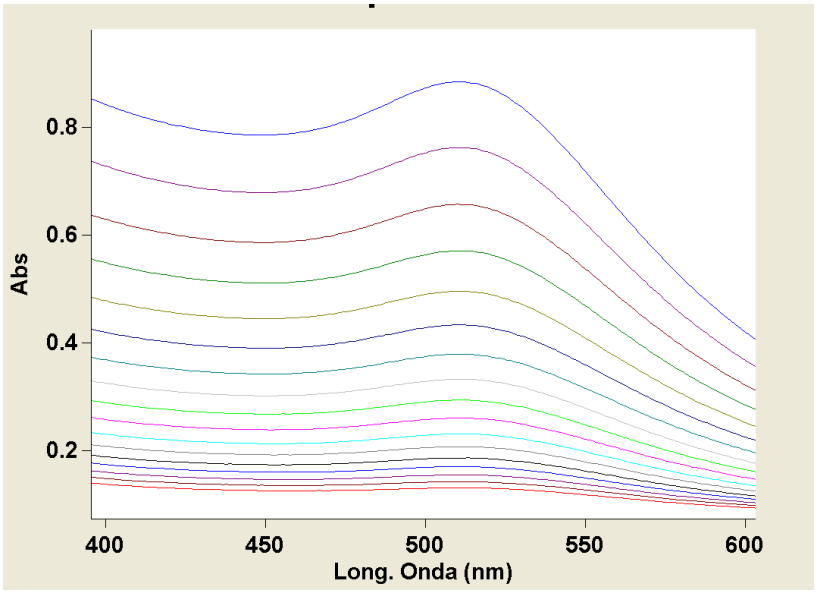

Figure B: UV-Vis absorption of **NP4** at different concentrations.

NP5: 75% HS-PEG-F and 25% HS-PEG-COOH

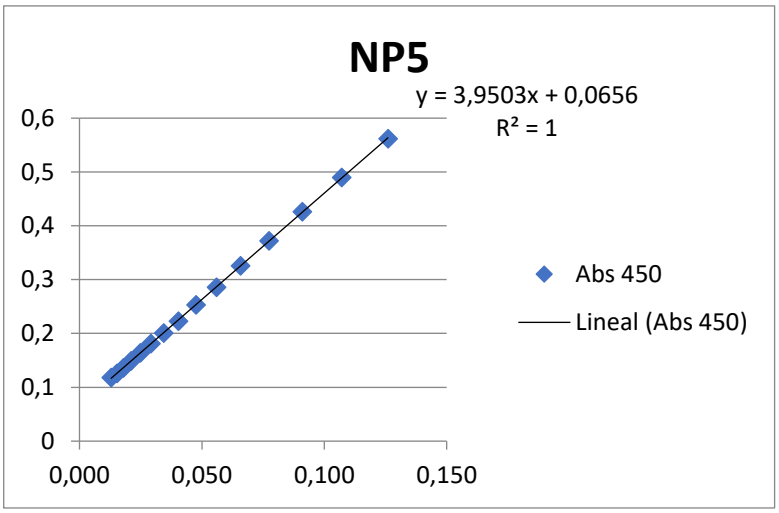

Graph C: Calibration line of **NP5**.

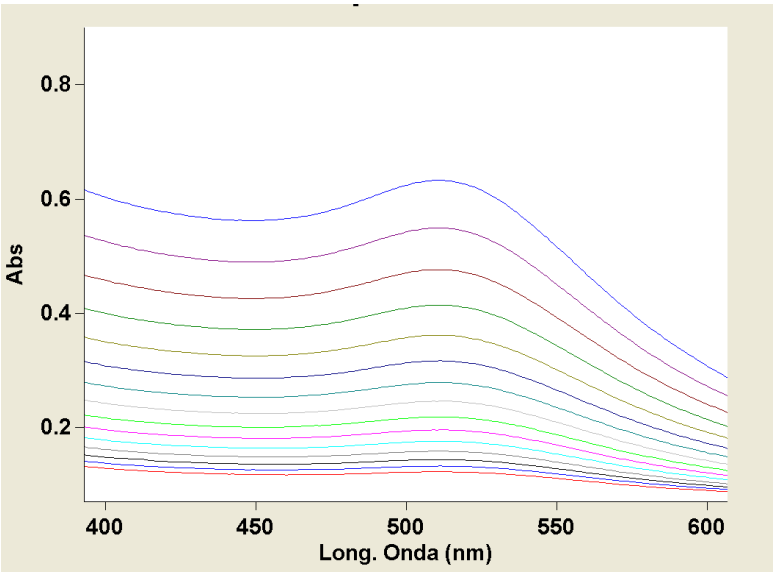

Figure C: UV-Vis absorption of **NP5** at different concentrations.

2. Batch's pictures

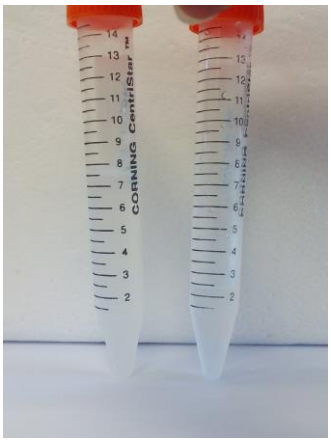

Figure D: Empty gelatin nanoparticles batch after purification at 2k (discarded) and 14k (suitable) from left to right.

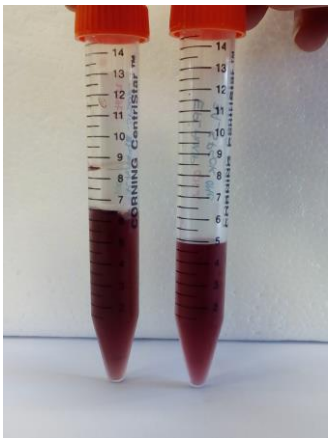

Figure E: Gold nanoparticles after purification **NP3** and **NP5** from left to right.

Figure F: Au-Gel2 nanoparticles batch at $6 \cdot 10^{-6}$ µmol NP4/mg gelatin after purification at 2k (discarded) and 14k (suitable) from left to right.

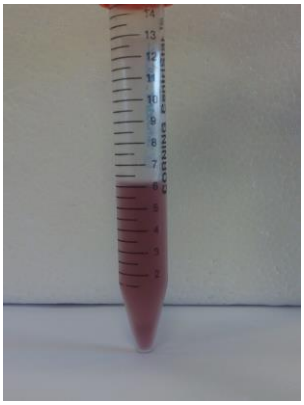

Figure G: Au-Gel2 nanoparticles batch at $12 \cdot 10^{-6}$ µmolNP4/mg gelatin after purification at 14 k (suitable).